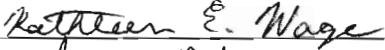
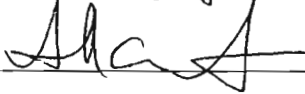


ACOUSTIC MODESHAPE INVERSION USING DEEP WATER
AMBIENT NOISE MEASUREMENTS

by

Khalid A. AlMuhanna
A Thesis
Submitted to the
Graduate Faculty
of
George Mason University
In Partial fulfillment of
The Requirements for the Degree
of
Master of Science
Electrical Engineering

Committee:

	Dr. Kathleen E. Wage, Thesis Director
	Dr. Jill K. Nelson, Committee Member
	Dr. Andre Manitius, Committee Member
	Dr. Andre Manitius, Chairman, Department of Electrical and Computer Engineering
	Dr. Lloyd J. Griffiths, Dean, The Volgenau School of Information Technology and Engineering

Date: June 4, 2008 Summer Semester 2008
George Mason University
Fairfax, VA

Acoustic modeshape inversion using deep water ambient noise measurements

A thesis submitted in partial fulfillment of the requirements for the degree of
Master of Science at George Mason University

By

Khalid A. AlMuhanna
Bachelor of Science
George Mason University, 2005

Director: Dr. Kathleen E. Wage, Associate Professor
Department of Electrical and Computer Engineering

Summer Semester 2008
George Mason University
Fairfax, VA

Copyright © 2008 by Khalid A. AlMuhanna
All Rights Reserved

Dedication

Dedicate to my parents, Norah and Abdulla
my sister Abrar, and brothers Abdulaziz, Meshari and Ahmed

Acknowledgments

I would like to thank God “Allah” for giving me a wonderful family that provides me with support and encouragement, ooh and for postponing one of my exams this semester :)

I am thankful for my loving parents Norah and Abdulla for all the free delicious home cooked food made by mom, and for also providing free housing. Some of the money I saved on rent sadly went to Caribou coffee and Starbucks.

Let’s not forget my siblings, sister Abrar, brothers Abdulaziz, Meshari and Ahmed; I am thankful for having you all in my life and for your support.

I would like to thank my advisor, Dr. Kathleen Wage for providing me with the opportunity to work with her on this project and introducing me to the world of research, which led me to giving a presentation at a workshop and finishing this thesis. I appreciate you being patient with me throughout my work on this thesis, and hope to continue working with you now that I know what I’m doing. I would also like to thank my committee members, Dr. Andre Manitius and Dr. Jill Nelson for accepting to be my committee members.

A thank you goes to my lab mates, Tarun Chandrayadula, Richard Wheelock, and Songshun Xu for their help and feedback on my thesis, and for the many interesting discussions.

A special thanks goes to my friends since Highschool for all their support throughout my studies Badr AlBawardy (my cuz), Ali AlFaiz, Khalid AlAssaf, Fahad AboTaleb who just started working back in Saudi, Mansoor AlBarrak, and Omar Alrashed.

I gratefully acknowledge financial support from the following sources: Office of Naval Research Grant N00014-05-1-0639, and the Saudi Arabian Cultural Mission.

Table of Contents

	Page
List of Figures	vii
Abstract	ix
1 Introduction	1
1.1 Acoustic Tomography & Normal Modes	1
1.2 Motivation	3
1.3 Previous Work	4
1.4 Goals	5
1.5 Organization	6
2 Background & Previous Work	7
2.1 Problem Statement	7
2.2 Background	8
2.2.1 Modes in the Ocean Channel	9
2.2.2 Ambient Noise	13
2.3 Previous work	14
2.3.1 Wolf <i>et al.</i> (IEEE Oceans 1993)	14
2.3.2 Neilsen and Westwood (IEEE Oceans 1993)	16
2.3.3 Hursky <i>et al.</i> (IEEE Oceans 1993)	17
2.3.4 D'Spain <i>et al.</i> (Pure appl. geophys, 2001)	19
2.4 Summary	19
3 Simulation	21
3.1 Narrowband Model	21
3.2 Array Span	25
3.3 Snapshot Problem	28
3.4 Array Tilt	32
3.5 Filter Design	39
3.6 Summary	42
4 Experimental Results (SPICE04)	44

4.1	SPICE04 overview	44
4.2	SPICE04 SVLA setup	45
	4.2.1 Setup	45
	4.2.2 Receptions	47
	4.2.3 Preprocessing	49
4.3	SPICE04 Noise	50
4.4	Noise Modeshapes	51
	4.4.1 Good Extraction	53
	4.4.2 Bad Extraction	56
4.5	Summary	61
5	Conclusion	62
	5.1 Concluding comments	62
	5.2 Future work	64
	Bibliography	66

List of Figures

Figure	Page
1.1 The Sound Speed Profile from the WOA database	2
1.2 The sound speed profile and the first 10 modes at 10 Hz and 40 Hz .	3
2.1 The sound speed profile and the first 10 modes at 10 Hz and 40 Hz .	12
3.1 Extracted modes using narrowband modes at 11 Hz as input	23
3.2 Correlation figure between the empirical modes and the ideal modes from Figure 3.1	24
3.3 Extracted modes using narrowband modes at 11 Hz as input	26
3.4 Correlation figure between the empirical modes and the ideal modes from Figure 3.3	26
3.5 Extracted modes using narrowband modes at 32 Hz as input	27
3.6 Correlation figure between the empirical modes and the ideal modes at 32 Hz with a VLA that spans depths 350 m to 1715 m with 35 m spacing between elements	27
3.7 Correlation image plot and plots of the simulated modes using a VLA that spans depths from 1 m to 5000 m with 35 m spacing, simulated using different snapshots	30
3.8 Correlation image plot and plots of the simulated modes using a VLA that spans depths from 350 m to 1715 m with 35 m spacing, simulated using different snapshots	31
3.9 VLA setup in simulation	33
3.10 Detailed tilt	34
3.11 Plots of the tilt at different angles of a water column spanning VLA with spacing of 35 m between elements	35
3.12 Correlation and a plots of the simulated modes of a tilted VLA from depths 1 m to 5000 m with 35 m spacing	36

3.13	Plots of the tilt at different angles of the VLA that spans depths from 350 m to 1715 m with spacing of 35 m between elements	37
3.14	Correlation and a plots of the simulated modes of a tilted VLA from depths 350 m to 1750 m with 35 m spacing	38
3.15	Correlation across frequency of modes 1 and 10	40
3.16	Magnitude and Phase of a Blackman window	41
4.1	A map showing the SPICE04 SVLA position	46
4.2	SVLA receivers shown relative to the SSP	47
4.3	SPICE04 SVLA setup	48
4.4	Block diagram showing the preprocessing steps for extracting the normal modeshapes	49
4.5	Ambient noise PSD over time at hydrophones 1, 20, and 39	52
4.6	Averaged noise PSD over time at hydrophones 1, 20, and 39	53
4.7	Averaged noise PSD over at hydrophones 20 and 39, zoomed in	54
4.8	Modeshapes of modes 1, 2, 3, and 5 over frequency for yearday 455	55
4.9	Modeshapes and correlation at a center frequency of 11 Hz for yeardays 347, and 401	57
4.10	Modeshapes and correlation at a center frequency of 11 Hz for yeardays 455 and 491	58
4.11	Modeshapes and correlation at a center frequency of 11 Hz for yeardays 407 and 431	59
4.12	The PSD at hydrophone 1 for 4 yeardays	60

Abstract

ACOUSTIC MODESHAPE INVERSION USING DEEP WATER AMBIENT NOISE MEASUREMENTS

Khalid A. AlMuhanna, Master of Science

George Mason University, 2008

Thesis Director: Dr. Kathleen E. Wage

Ocean acoustic tomography is a powerful method that uses sound to study ocean properties such as temperature, which is directly related to sound speed in water. This thesis focuses on using ambient noise to infer the normal modes of the ocean waveguide. The modes are a set of orthogonal functions that are solutions to the depth dependent wave equation, which depends on sound speed and thus on the temperature. Assuming that noise signals received by a vertical array consist of a sum of uncorrelated modes, the modeshapes can be determined from an eigenvector decomposition of the measured cross-spectral density matrix. Several authors have applied this technique to estimate the modes of shallow water waveguides, but there have been few opportunities to apply this technique in deep water waveguides. In this thesis the modeshapes of a deep water environment in the North Pacific are estimated using ambient noise data measured during the SPICE04 experiment. Although noise measurements were not the primary focus of SPICE04, the experiment provided a large data set for this analysis. In addition to acoustic measurements, the experiment also included extensive sampling of the environmental parameters. This thesis

summarizes some of the noise statistics measured during 2004-2005. The measured modeshapes derived from the data are compared with the true modes derived from the measured environmental data.

Chapter 1: Introduction

1.1 Acoustic Tomography & Normal Modes

Ocean acoustic tomography is a powerful method that utilizes sound to study the properties of the medium, such as temperature. One example is travel time tomography, where measurements of travel time are used to infer sound speed, which is directly related to ocean properties [1]. The speed of sound underwater, not surprisingly, depends on the characteristics of the water. For example the speed of sound in sea water increases as the temperature increases, but it is also affected by the pressure and the salinity of the water. By measuring these properties over a water column at a certain time it is possible to generate a profile of the depth dependent speed of sound, called the Sound Speed Profile (SSP). Figure 1.1 shows a typical deep water SSP for a 5000 m waveguide, generated from the World Ocean Atlas data. The World Ocean Atlas (WOA) is a database of the temperature and salinity measurements that can be converted to construct the SSP [2].

In the deep water environment (deep water in this thesis refers to a water column that is around 5000 m deep) signals propagate around an axis called the acoustic channel axis. The channel axis is the point with the minimum sound speed in Figure 1.1, which is typically at depths around 700 m to 1000 m. When sound waves propagate through the ocean medium they oscillate around the channel axis. The way they oscillate is by refraction, which means when a signal is propagating from the bottom to the surface it is refracted back to the bottom and the same occurs when the signal reaches the bottom.

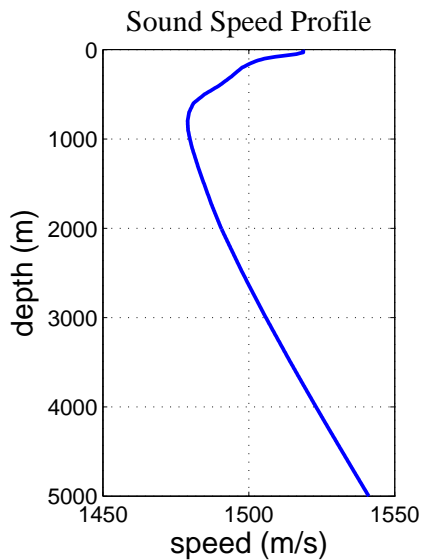


Figure 1.1: The sound speed profile averaged over time from the World Ocean Atlas database [2].

As acoustic signals propagate through the ocean, standing waves are created by constructive and destructive interferences. These standing waves are the normal modes of the ocean medium. The shapes of the modes depend on the shape of the SSP and on the frequency of the source. A certain mode has different shapes at different frequencies. Figure 1.2 shows the SSP and the first 10 modes at different frequencies. The solid blue lines represent the modes at 10 Hz and the red dashed lines represent the modes at 40 Hz. From the figure, the difference between the modes at 10 Hz and 40 Hz is very clear. As the frequency increases the modeshapes become more compact in depth.

The received pressure field at a certain location can be represented as a sum of scaled normal mode functions. Theoretically it is possible to make measurements across depth over the water column, using a Vertical Line Array (VLA) of receivers, and extract the normal modeshapes from the measurements. The pressure field, measured using a VLA, at a certain location depends on the SSP by the depth dependent

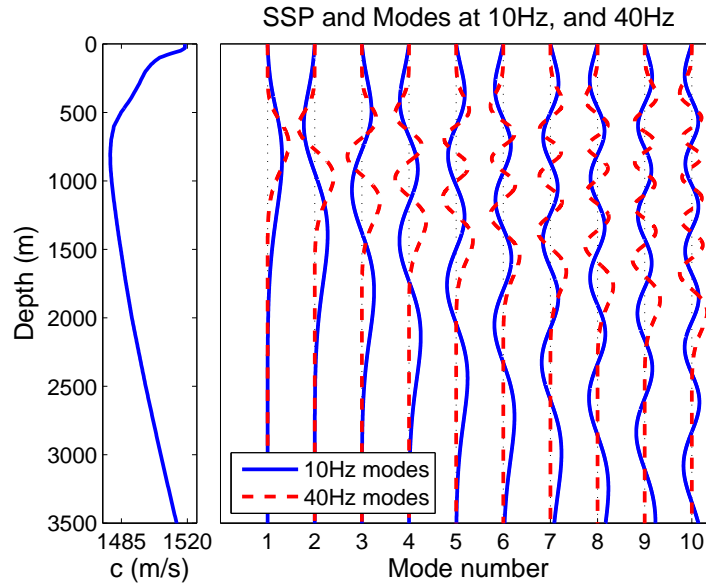


Figure 1.2: The sound speed profile (left subplot) and the modeshapes (right subplot) for a typical deep water environment. The solid blue lines are the modeshapes at 10 Hz and the red dashed lines are the modeshapes at 40 Hz.

acoustic normal mode functions. The normal modes are a set of orthogonal functions that are solutions to the depth dependent wave equation, which depends on the SSP (discussed more in Chapter 2).

1.2 Motivation

The main goal of this thesis is to extract the modeshapes from receptions of ambient noise underwater made during the SPICE04 experiment conducted by the North Pacific Acoustic Laboratory (NPAL) group. Although noise measurements were not the primary focus of SPICE04, the experiment provided a large data set, about 6 months, of pressure field measurements for this analysis. In addition to acoustic measurements, the experiment also included extensive sampling of the environmental parameters, which makes it possible to compute the actual SSP any time

during the experiment. SPICE04 provides an opportunity to study the ambient noise modeshapes and compare them to the actual modeshapes in deep water, which is the main motivation for this thesis.

For many years there has been work on simplifying the extraction of modeshapes from measurements of the pressure field across a VLA, which uses eigendecomposition of the Cross-Spectral Density Matrix constructed from the measured pressure field. It has been shown in past experiments that it is possible to extract modeshapes when there is a known source present, and without knowledge of the environmental parameters [3]. An acoustic source at a certain frequency can excite the modes at that frequency and hence the modeshapes at that frequency can be extracted from the receptions of the pressure field containing the transmitted acoustic signal. Most work done so far was done in shallow water environments. There has been very little work on trying to estimate the modeshapes from measurements of ambient noise, especially in deep water environments.

1.3 Previous Work

This section presents a brief overview of the previous work relevant to this thesis. Most previous work on estimating the modeshapes is applied in shallow water. For this thesis, shallow water refers to depths less than 300 m. There are few experiments related to the work presented in this thesis, and the most notable ones are reviewed in Chapter 2.

We believe Wolf *et al.* were the first to use the method discussed in this thesis for extracting the modeshapes from measurements of the pressure field. The authors were able to extract the modes from a controlled source in very shallow water around 18 m deep [4]. Neilsen and Westwood studied experiments conducted in a water

column that is about 70 m deep with controlled sources and one of the experiments was without a source (*i.e.*, ambient noise receptions) [3]. The authors demonstrated the extraction of the modes in all experiments including the one with ambient noise receptions. Hursky *et al.* were able to extract both the wavenumber and the modeshapes using a VLA that spanned the bottom 118 m of a 212 m deep water column of receptions from a controlled source [5]. In the fourth paper by D'Spain *et al.*, they had an array that spanned the top 3000 m with 200 elements, which was deployed in a 5160 m deep water column. In that paper they were able to extract the modeshapes from earthquake T-phase arrivals successfully. Chapter 2 discusses these papers in more detail.

There are some good reasons that most previous work is implemented in shallow water environments. In shallow water it is easy to sample the whole water column, because a small number of sensors is needed to span the water column. In deep water environments it is difficult and expensive to deploy enough sensors to span the water column. The effects of array motion on the receptions from a VLA in shallow water are small compared to the effect on the receptions from a VLA in deep water. Ocean waves can cause the VLA to tilt in both shallow water and deep water environments. The affect of tilt on the pressure field receptions in deep water environments is greater due to the length of the VLA. In terms of processing for modeshapes, shallow water environments support fewer propagating modes than deep water.

1.4 Goals

The main goal of the thesis to extract the modeshapes from ambient noise measurements made during the SPICE04 experiment. Prior to extracting the modeshapes simulations are needed to test the limitations of the eigendecomposition approach in

a controlled environment. The goal of the simulations is to examine the effects of parameters such as the span of the VLA, frequency, and tilt of the modeshape extraction for a deep water environment. The ambient noise measured throughout the SPICE04 experiment is analyzed as well.

1.5 Organization

The organization of the thesis is as follows. Chapter 2 presents background information on the ocean environment and mode estimation, along with a detailed description of previous work on the estimation of normal modes. Simulation and analysis of the performance of the modeshape extraction method is presented in Chapter 3. Chapter 4 discusses the SPICE04 experiment and analyzes the results of the modeshape extraction from data. Chapter 5 concludes the thesis and discusses future work.

Chapter 2: Background & Previous Work

The main goals of this chapter are to present a mathematical definition of the problem addressed in this thesis and to review previous work. A part of the chapter includes a detailed definition of the normal mode functions, and how they add up to make the pressure field of the water column. The first section addresses the main problems presented in this thesis and what is achieved in this work. Section 2.2 describes the ocean model and how modes are related to signals propagating through the ocean from a source to a receiving VLA, and provides a description of the sources of ambient noise in an underwater environment. Section 2.3 reviews the previous work on estimating modeshapes in ocean waveguides.

2.1 Problem Statement

As stated in Chapter 1, the problem with most VLAs deployed in deep water environments is that it is very difficult to make measurements of the environmental parameters, such as temperature and salinity, for the entire period that the array is deployed. If such environmental data is available, the SSP can be constructed and used to calculate the modeshapes. If not, an archival SSP must be used for mode calculations. The likelihood that the archival data are taken at the same times and location of the VLA studied is very small, which could lead to errors. Fortunately previous work in shallow water indicates that it is possible to invert for the environmental parameters using only the extracted modeshapes from the received pressure field without any knowledge of the environmental parameters [3,6].

It is uncertain if it is possible to invert for the SSP in cases where we have a VLA in a deep water environment. Therefore this thesis focuses on the first step prior to inverting for the SSP, which is extracting normal modeshapes using ambient noise measurements in a deep water environment. The ambient noise measurements used in this thesis were made during the SPICE04 experiment. The experiment was a part of larger project conducted by the North Pacific Acoustic Laboratory (NPAL) group, and is discussed in more detail in chapter 4. Because array motion, primarily tilt, is a major problem to deal with when using VLAs, it is very important to take into account the affects of a tilted array on the extracted modeshapes. If there is a source present at a known location from the VLA, array tilt can be easily corrected for to improve the signal to noise ratio of the received signal. Ambient noise comes from every direction around the array, which makes it not possible to correct for array tilt of the VLA receptions processed in this thesis.

Fortunately during the SPICE04 experiment extensive sampling of the environmental parameters were taken during the course of the experiment. This allows for the SSP to be generated and thus the actual modeshapes calculated at that location. Since the actual modeshapes can be calculated during the experiment, it is possible to test the method used in previous work to extract the modeshapes in deep water environments. This thesis compares the extracted modeshapes from ambient noise measurements made during the experiment to the actual modeshapes calculated from the environmental measurements.

2.2 Background

As stated in Chapter 1, normal modes are standing waves in depth that can be used to describe the pressure field associated with propagating signals. The normal

modes present at a certain location and time should theoretically be the same as the modes calculated using the solution of the wave equation defined below [7]

$$\frac{1}{r} \frac{\partial}{\partial r} \left(r \frac{\partial p}{\partial r} \right) + \frac{\partial}{\partial z} \left(\frac{\partial p}{\partial z} \right) + \frac{\omega^2}{c^2(z)} p(r, z) = -\frac{\delta(r) \delta(z - z_s)}{2\pi r}, \quad (2.1)$$

where the variables are defined as follows:

r : is the horizontal range between source and receiver;

z : is the depth of the receiving element;

z_s : is the source depth;

p : is the pressure field at range r and depth z ;

$c(z)$: is the depth dependent sound speed profile;

ω : is the frequency.

The most effective way to capture the depth dependent mode functions is by deploying a VLA that samples the shapes of the modes across depth. Section 2.2.1 describes mathematically how the modes can be extracted using measurements recorded with a VLA. A discussion of the sources of underwater ambient noise is contained in section 2.2.2.

2.2.1 Modes in the Ocean Channel

The solution to the wave equation (2.1) can be written as a sum of normal modes, that is,

$$p(r, z) = \sum_{m=1}^{\infty} a_m(r) \phi_m(z), \quad (2.2)$$

where:

$a_m(r)$ is a complex amplitude of each mode function at range r ;

$\phi_m(z)$ are the depth dependant mode functions at depth z .

The depth dependent mode functions $\phi_m(z)$ are the solutions to the differential equation given by the equation below:

$$\frac{d^2\phi_m(z)}{dz^2} + \left(\frac{\omega^2}{c^2(z)} - k_m^2 \right) \phi_m(z) = 0 , \quad (2.3)$$

where k_m is the wave number at a certain frequency of the m^{th} mode. The depth-dependent mode functions are an orthogonal basis set of functions $\phi_m(z)$ such that¹

$$\int_0^D \phi_n(z)\phi_m(z)dz = \begin{cases} 1 & \text{for } n = m \\ 0 & \text{for } n \neq m \end{cases} \quad (2.4)$$

In order to extract these modeshapes, measurements of the pressure field over the depth of the water column need to be made. A VLA of sensors is a method to make measurements at different depths of the water column at the same time. In general the sensor elements used to measure pressure under water are referred to as hydrophones, which are underwater microphones. The pressure field is represented by receptions of acoustic signals from a source at range r using N hydrophones in the VLA at depths $z_1, z_2, z_3, \dots, z_N$. The pressure field \mathbf{p} has depth dependent elements

¹For simplicity the density is assumed to be unity in the thesis.

and can be written as a vector:

$$\mathbf{p} = \begin{bmatrix} p(z_1, r) \\ p(z_2, r) \\ \vdots \\ p(z_N, r) \end{bmatrix}. \quad (2.5)$$

The underwater acoustic pressure field elements can be represented as a scaled sum of the orthogonal set of the normal modes at those depths. The depth dependent M modes can be combined and represented in a matrix form by the matrix Φ as

$$\Phi = \begin{bmatrix} \phi_1(z_1) & \phi_2(z_1) & \cdots & \phi_M(z_1) \\ \phi_1(z_2) & \phi_2(z_2) & \cdots & \phi_M(z_2) \\ \vdots & \vdots & \cdots & \vdots \\ \phi_1(z_N) & \phi_2(z_N) & \cdots & \phi_M(z_N) \end{bmatrix} = \begin{bmatrix} \phi_1(z) & \phi_2(z) & \cdots & \phi_M(z) \end{bmatrix}, \quad (2.6)$$

where the columns represented by $\phi_1(z), \phi_2(z), \dots, \phi_M(z)$ are the depth-dependent modes ordered from lowest (1) to highest (M). A set of modes calculated by solving the differential equation (2.3) using a given SSP from the World Ocean Atlas (WOA) database is shown in Figure 2.1 [2]. One easy way to tell which mode is which is by looking at the shape of the mode as seen in the figure, mode 1 has one “hump”, mode 2 has two “humps”, and so on. The first 10 modes at 10 Hz and 40 Hz with their corresponding SSP are shown in the figure. It is clear from the figure that the shape of the modes depends not only on the SSP, but also on frequency. As the frequency increases the more compact the modes are in depth around the

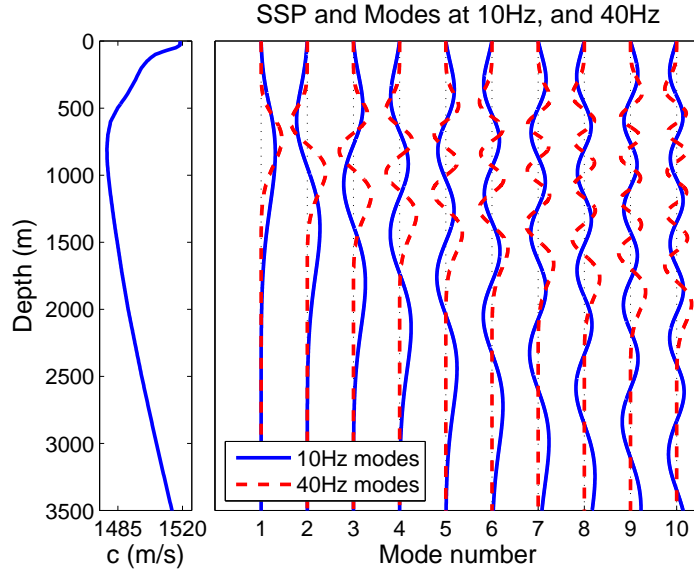


Figure 2.1: The sound speed profile (left subplot) and the modeshapes (right subplot) for a typical deep water environment. The solid blue lines are the modeshapes at 10 Hz and the red dashed lines are the modeshapes at 40 Hz.

minimum sound speed.

The expression of the acoustic pressure field represented in equation (2.2) is rewritten in matrix notation as

$$\mathbf{p} = \mathbf{\Phi} \mathbf{a} , \quad (2.7)$$

where:

$\mathbf{\Phi}$ is as defined in equation (2.6);

\mathbf{a} is a vector of complex amplitudes of the modes.

The modeshapes in $\mathbf{\Phi}$ can be extracted from the received pressure field by constructing

the Cross-Spectral Density Matrix (CSDM) \mathbf{R} , in the equation below.

$$\begin{aligned}
\mathbf{R} &= \mathcal{E} \{ \mathbf{p}\mathbf{p}^H \} = \mathcal{E} \{ \Phi \mathbf{a}\mathbf{a}^H \Phi^H \} \\
\Rightarrow \mathbf{R} &= \Phi \mathcal{E} \{ \mathbf{a}\mathbf{a}^H \} \Phi^H \\
\Rightarrow \mathbf{R} &= \Phi \mathbf{R}_a \Phi^H ,
\end{aligned} \tag{2.8}$$

where $\mathbf{R}_a = \mathcal{E} \{ \mathbf{a}\mathbf{a}^H \}$. The final line in equation (2.8) looks very similar to the definition of eigendecomposition of \mathbf{R} in the equation below.

$$\mathbf{R} = \mathbf{V}\mathbf{D}\mathbf{V}^H , \tag{2.9}$$

where \mathbf{V} is a matrix containing the eigenvectors of the matrix \mathbf{R} . The matrix \mathbf{D} is a diagonal matrix containing the eigenvalues of the CSDM \mathbf{R} . It is now possible to see that the empirical modes $\hat{\Phi} = \mathbf{V} \approx \Phi$.

2.2.2 Ambient Noise

Ambient noise underwater is a combination of the sounds of which the source, range and location of each source cannot be identified. Any background noise existing underwater can be thought of as ambient noise [8]. Underwater noise can vary from one location to another in the ocean. Ambient noise also varies as a function of depth.

One source of ambient noise is marine mammals such as whales and dolphins. Other sources of noise are rain drops hitting the surface of the ocean and the speed of wind or wind stress on the surface of the ocean. Wind stress cause the waves to break at the surface of the ocean, which cause clouds of bubbles that produce noise when the clouds oscillate [9]. Anthropogenic sources also contribute to the ocean's noise, mainly from the noise created by shipping traffic, which represents a large portion of

the overall ambient noise.

Different sources contribute to different parts of the spectrum, *i.e.*, emit sounds at different frequencies. For example fish and shrimp generate sounds at frequencies from 20 Hz up to hundreds of kilohertz [10]. Marine mammals such as dolphins emit acoustic ‘clicks’ with frequencies ranging from 1 kHz to about 130 kHz [11]. Other sources such as rain generate noise at frequencies between 1 kHz to 50 kHz [10]. The spectrum underwater during heavy rain is described as “white” by [8]. In deep water, shipping traffic usually dominates the spectrum of ambient noise, where the frequency band for distant shipping traffic ranges from 10 Hz to about 200 Hz [9].

There has been research done on modeling underwater acoustic noise of the stratified ocean. A notable contribution is the wind driven noise model introduced by Kuperman and Ingenito [12]. Their model uses the normal modes to generate the spatial spectrum of noise. Their initial model was for two dimensions, but with other collaborators they extended their results to a three dimensional model [13].

2.3 Previous work

The technique of extracting acoustic normal modes from pressure measurements without prior knowledge of the environment has been implemented in experiments by several research groups. This section presents a brief overview of the work that is relevant to this thesis. The first three papers describe experiments in shallow water environments. The fourth paper discusses a deep water experiment.

2.3.1 Wolf *et al.* (IEEE Oceans 1993) [4]

Wolf *et al.* constructed spatial filters for normal modes in a shallow water environment. We believe that they were the first to suggest extracting the modes

using eigendecomposition of the CSDM. The beginning of the paper discussed finding a simple way to extract normal modes from pressure field measurements [4]. They started with equation (2.2) and said that pressure \mathbf{p} from equation (2.5) can be represented as equation (2.7).

According to the authors, if the VLA does not span (*i.e.*, sample) the whole water column then the orthogonality condition for the modes does not apply. This means that if there aren't enough hydrophones that are closely spaced together from the surface to the bottom of the water column, then it may not be correct to represent the pressure field as in equation (2.7). Now that the pressure field is represented, they were able to extract the modeshapes of a narrowband signal from measurements of the pressure field, by using equations (2.8), and (2.9)

The experiment that was discussed in this paper consisted of a VLA that stood in a water column that was 18 m deep with an aperture of 16.4 m that was deployed from the Naval Ocean Systems Center Oceanographic Tower. The VLA was made up of 25 hydrophones equally spaced across the array. A source transmitting acoustic signals was anchored on a vessel 3.7 km away from the receiving array. Eigenanalysis was performed on the received signals and the authors were successful in extracting the modeshapes.

Wolf *et al.* stated some ground rules for estimating the modeshapes when using a VLA that partially spanned the water column. The main one was, if an array only partially spans the water column then the depth dependent normal modes captured by the array will be only linearly independent, where the eigenvectors of \mathbf{R} are always orthogonal [4]. In those cases it is not possible to extract the exact modes using eigenvector decomposition [4].

Wolf *et al.* found that the extracted modes in their experiment had the same shape of the calculated normal modeshapes. Their extracted modes were not smooth

but had a similar shape as the calculated modeshapes. Overall their results show that it is possible to get the modeshapes using eigendecomposition.

2.3.2 Neilsen and Westwood (IEEE Oceans 1993) [3]

Neilsen and Westwood presented work on the extraction of the depth dependant mode functions using VLA receptions in an underwater environment. This work led to Neilsen's PhD dissertation [6], which presented the work in the paper in more detail. This paper considers three different scenarios. The first is when there is a source transmitting continuous wave signals at a range r that is moving away from the receiving array, in a range independent track, where there was constant bathymetry. The second is when the source is also moving away from the array in a range dependant track, where the ground floor of the water column is sloping up as the source moves away from the VLA. The final scenario was conducted when the source is turned off, *i.e.*, ambient noise measurements of the pressure field were recoded by the VLA.

Neilsen and Westwood used a slightly different method to extract the modes, where they noted that the modeshapes can be extracted from the Singular Value Decomposition (SVD) of the pressure field in vector form as received by the VLA. This method is very similar to that described in the Wolf *et al.* paper, because the elements in the SVD are the eigenvectors and the eigenvalues matrices of the CSDM \mathbf{R} in equation (2.8).

According to Neilsen's thesis, to be able to extract modeshapes there are a set of requirements needed for the experiment [6]. The first was the same as the previous paper, *i.e.*, that the array must span the complete water column and have densely spaced sensors that sample the complete modeshapes [6]. The second requirement is that the sources should be strong enough to make the signal go through the interval

between source and receiver without much loss [6].

The VLA used in this work spanned 73 m using 20 elements with variable spacing between elements. The elements of the VLA were closely spaced towards the bottom of the water column, with a spacing of about 2 m, and more widely spaced (about 7.6 m) near the top of the array (*i.e.*, the surface of the water) [3]. The authors warn that this is not a good design for a VLA to extract depth dependent normal modes [3]. In both, the range-dependent and the range-independent tracks the authors were able to extract the modes successfully when the source transmitted signals with center frequencies at 100, 150, and 200 Hz.

In the experiment there was a run when the VLA was recording while the source wasn't turned on. The source was on a ship at least 22 km away from the receiving array. The authors implemented the SVD method to extract the modes of the ambient noise measurements at frequencies of 120, 250, and 350 Hz, and their results were very close to the true modes [3].

According to the authors many of the modes extracted from the ambient noise measurements had a high correlation to modeled modes from a measured SSP [3]. For the purpose of this thesis it was very helpful to know that it is possible to get an estimate of the modeshapes from measurements of just ambient noise.

2.3.3 Hursky *et al.* (IEEE Oceans 1993) [5]

Hursky *et al.* in this work used data derived modes to implement Matched Field Processing (MFP). They claimed that it is very difficult to do much with estimated modes, and that both the wavenumbers and the modeshapes are needed for implementing MFP [5]. The data used in this paper was from the SWellEx-96 experiment. The method used to extract an estimate of the normal modes is very similar to

the method used in the Wolf *et al.* paper, in the sense that they used eigenvector decomposition of the CSDM of the pressure field \mathbf{p} like in equations (2.2), and (2.8). To achieve the goal of obtaining the wavenumbers, the authors used a measured SSP that was made during the experiment. The authors then used a method to extrapolate the wavenumbers, which is referred to as the Shooting method [5]. More information on the shooting method can be found in [7](section 5.7).

For the purpose of the thesis we are only concerned with the part of the paper that is involved with estimating the modeshapes using receptions from the SWellEx-96 experiment. A VLA of 64 equally spaced elements that only spanned the bottom part of a 212 m deep water column that started at 94 m to the bottom. There were three main parts of the experiment, all of which had a moving sources. The first was with a source about 8 to 9 km, which moved towards the VLA to a range of about 3 to 4 km away. In the second part, the source moves closer to the receiving array in the same direction as in the first part. The source moves from about 3 km away from the VLA then gets to a range of about 1 km away, and then moves about 3 km away from the source. The third part of the experiment is with a source located at about 3 km away from the VLA and moves away and up-slope from the receiver to about 9 km away, with the depth of the water column ranging from 200 m to about 100 m.

The method for extracting an estimate of the modes was possible with the source transmitting tones over the range of 49 Hz to 488 Hz. They were able to extract some modeshapes from the receptions. Hursky *et al.* found that fewer modes were extracted at higher frequencies. Their logic for that is for a number of reasons, the first being that their array only spanned half of the water column. The second is that at higher frequencies a greater number of modes are propagating. Their third thought is that the spacing between wavenumbers decreases at higher frequencies, which makes it harder to estimate the modes using eigenvector decomposition of the

CSDM, unless the source was far enough for the modes to become uncorrelated [5]. The latter is a key point to keep in mind for the work presented in this thesis.

2.3.4 D’Spain *et al.* (Pure appl. geophys, 2001) [14]

D’Spain *et al.* analyzed earthquake T-phase receptions using a VLA in a deep water column. The array used in the experiment was the Long Vertical Line Array (LVLA), which spanned the top 3000 m of the water column using 200 equispaced receiving elements. The authors used the arrivals of T-phase signals generated from earthquakes as signals that probe the ocean to the array position. They studied the differences between earthquakes originating on land and underwater. They were able to extract the modeshapes from the T-phase receptions at relatively low frequencies, around 5 Hz.

The depth of the water column in this experiment is very close to the depth of the water column considered in this thesis. The earthquake T-phase signals were not a controlled source, and the authors had some knowledge of the strength of the earthquakes and from which direction the signals were coming from. Even though the array used in this paper was longer and uses some sort of source, their results sheds the light even more that it is possible to extract the modeshapes in deep water environments.

2.4 Summary

Previous results show that it is possible to represent the acoustic underwater pressure using equation (2.7). Both methods, either by using SVD or by performing an eigenanalysis of the CSDM of the pressure field measurements, extract the eigenfunctions of the CSDM. The last paper by D’Spain *et al.* indicates that it is possible

to extract normal modes in a deep water environment, which is relevant to the scope of this thesis. The main question when extracting the modeshapes is, how do we know that these are the right shapes? What is needed is a metric that checks how close the extracted modeshape is to the ‘actual’ modeshapes extracted from the solutions of the partial differential equation of the pressure in equation (2.1). A proposed metric is presented in Chapter 3.

Chapter 3: Simulation Results

The main goal of this chapter is to present simulations that test the performance of the mode extraction method proposed in Chapter 2. Simulations of the pressure field are implemented and the extracted modes are shown. The limitations of the array (*i.e.*, array tilt) on the extraction of the modeshapes is tested in simulations as well. The first section discusses the approach to simulating the narrowband pressure field for an ideal VLA (*i.e.*, water column spanning VLA) in a controlled environment. Section 3.2 discusses the limitations of the VLA, such as spacing between elements and the span of the array. The number of snapshots required to generate a good CSDM for mode extraction is studied in section 3.3. Section 3.4 discusses the impact of array tilt on the VLA pressure field receptions of noise. The design of the best narrowband filter for this application is discussed in section 3.5.

3.1 Narrowband Model

This section presents simulations of the pressure field using the narrowband modeshapes to generate the pressure field as stated in the previous chapter. As noted in Chapter 2, the modes are frequency dependent, so the narrowband model will use modes at a single frequency to generate simulations of the pressure field. The VLA in this section is assumed to be a perfectly vertical array that spans a water column that is 5000 m deep, and a spacing between elements of 35 m. The received pressure field receptions require no phase corrections or other adjustments. The pressure field

equation (2.7) from Chapter 2 is rewritten for simplicity:

$$\mathbf{p} = \Phi \mathbf{a} . \tag{3.1}$$

Recall that Φ is a matrix containing the modeshapes at a single frequency and \mathbf{a} is a vector of amplitudes for each of the modes. There are 2 main rules for extracting the modeshapes in an underwater environment, and they are similar to the ones in previous work [3–6]. The first one is that the array should densely sample the water column, and the second criteria is that the weight for each mode should be 5% to 10% different from the adjacent modes according to [3,6]. The latter criteria comes from linear algebra. According to Golub and Van Loan the eigenvalues have to be significantly different from one another in order for the associated eigenvectors to not be “wobbly” [15]. The closer the eigenvalues are to one another, then the closer the angle is between the associated eigenvectors. This limitation is used by the authors in [3] as a minimum criterion in order to get a good estimate of the modeshapes.

The ideal covariance matrix can be constructed directly by using equation (2.8) from Chapter 2, which is rewritten below for convenience.

$$\mathbf{R} = \Phi \mathbf{R}_a \Phi^H , \tag{3.2}$$

where \mathbf{R}_a is the covariance matrix of \mathbf{a} . Since this is an ideal situation we will assume that the noise is independent, which would make \mathbf{R}_a a diagonal matrix with the power of the weights for each of the modeshapes on the diagonal. The eigenvectors of the covariance matrix will be referred to as the empirical modes or the extracted modes. The simulation in Figure 3.1 shows the first 6 extracted modeshapes in solid blue lines and the ‘ideal’ modeshapes (*i.e.*, the modes used as input to equation (3.2)) in red dashed lines. The modes used in this simulation are the narrowband modes

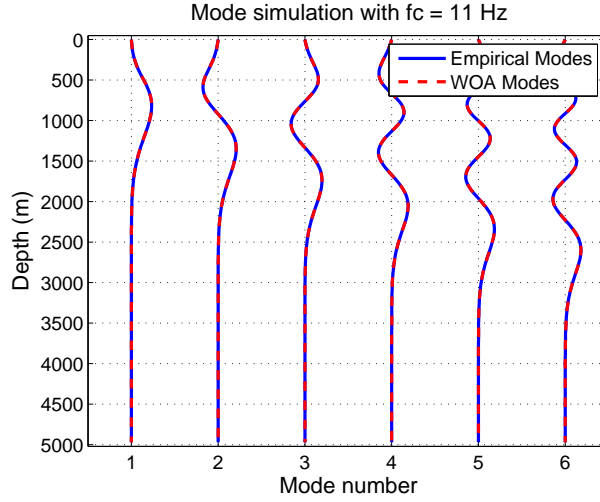


Figure 3.1: The extracted modes in solid blue lines and the input narrowband WOA modes at 11 Hz in red dashed lines. The simulation is created using an ideal (*i.e.*, spans depths from 1 m to 5000 m with 35 m spacing) vertical array.

of the WOA data set generated at 11 Hz, and the array is a 143 element array that spans depths from 1 m to 5000 m with a 35 m spacing between elements.

The empirical modeshapes look exactly like the original WOA modes, but a numerical comparison is useful. This thesis proposes a correlation metric for comparing the extracted modeshapes to the modeshapes from the WOA data or the actual modeshapes at the location of the array. The metric is the inner product between the extracted modeshapes and the WOA modeshapes, which is shown in the equation below.

$$\mathbf{C}_{corr} = \hat{\Phi}^H \Phi_{\text{WOA}} , \quad (3.3)$$

where $\hat{\Phi}$ is a matrix that contains the empirical modeshapes, *i.e.*, the obtained modeshapes from the eigendecomposition of the CSDM \mathbf{R} . Recall that $\hat{\Phi}$ is an N by M matrix, where N is the number of receivers and M is the number of modes. Φ_{WOA} is a matrix containing the normalized WOA modes and has the same dimensions as

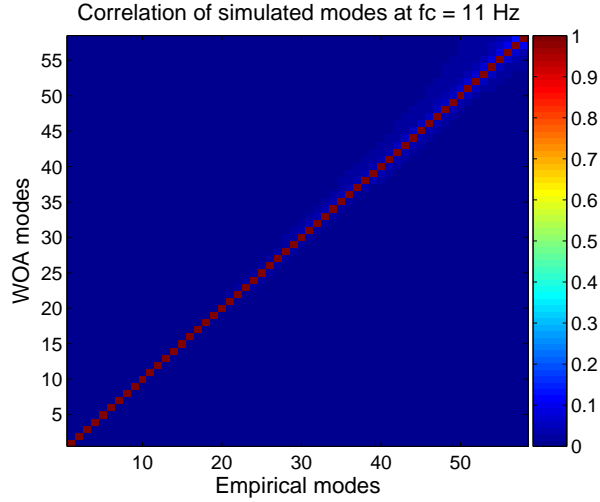


Figure 3.2: An image plot showing the correlation between the empirical modes and the ideal (input in this case) modes, where a 0 scale means they are not correlated and 1 means they are perfectly correlated.

$\hat{\Phi}$. The output matrix \mathbf{C}_{corr} is an M by M matrix, where the columns represent the correlation coefficient of the empirical modeshapes with the WOA modeshapes and vice versa for the rows. The correlation matrix is normalized and the absolute value is taken to obtain a correlation coefficient that is between 0 and 1.

When an ideal VLA is used, such as the VLA used in this section, a diagonal \mathbf{C}_{corr} is expected. Figure 3.2 shows the correlation matrix in an image scale plot of the empirical modeshapes versus the ‘ideal’ modeshapes. The scale represents the correlation coefficient (*i.e.*, scale from 0 to 1), where 0 means there is no correlation and 1 means there is perfect correlation. The correlation is almost a diagonal matrix of ones. As the mode numbers increase, the correlation decreases slightly to 0.987¹, because as the mode number increases the shape of the mode oscillates more, therefore it requires finer sampling in depth than every 35 m. If the array used had a 1 m spacing between elements then the correlation matrix would be perfectly diagonal.

¹This small decorrelation may be difficult to see in Figure 3.2.

3.2 Array Span

This section discusses the effect of the array aperture on the performance of the modeshape extraction algorithm. Full water column spanning arrays are not typically available. This section compares the results from a water column spanning VLA to the results from an array with the same aperture as the VLA used in the SPICE04 experiment, known as the Shallow VLA or SVLA. The simulated VLA used in this section has 40 elements with 35 m spacing, and spans depths from 350 m to 1715 m. The position of the array is carefully placed such that it is centered around the channel axis (*i.e.*, the minimum of the SSP). Similar to the previous section, the array is assumed to be perfectly vertical.

The empirical modeshapes and the input modeshapes from the WOA data set are shown in Figure 3.3 at 11 Hz. The simulation is generated using equation (3.2) from the last section, where the empirical modes are the eigenvectors of the CSDM \mathbf{R} . The empirical modeshapes are represented in the figure as blue solid lines and the WOA modeshapes are in the red dashed lines. The plots show that the modes look about the same for the first 2 modes, while the higher order modeshapes appear significantly different.

Figure 3.4 is an image plot showing the correlation coefficient values between the empirical modeshapes and WOA modeshapes. The correlation is generated the same as the correlation from the last section by using equation (3.3). From the correlation figure the modeshapes start off correlated for modes 1 and 2, then the correlation increases very fast as the mode number increases.

The array used in this section and throughout the thesis is a more practical array in real situations. The main reason this array performed poorly at 11 Hz is because the array was designed for higher frequencies. If the generated modes

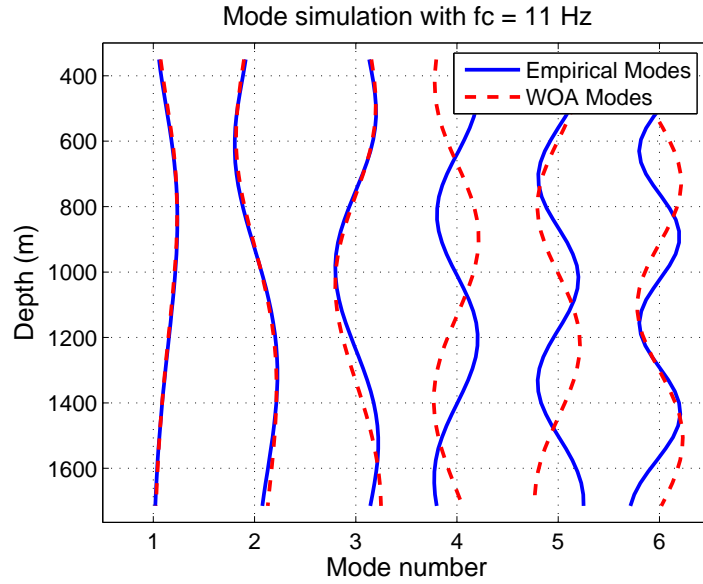


Figure 3.3: The extracted modes in solid blue lines and the input narrowband WOA modes at 11 Hz in red dashed lines. The simulation is created using the SVLA.

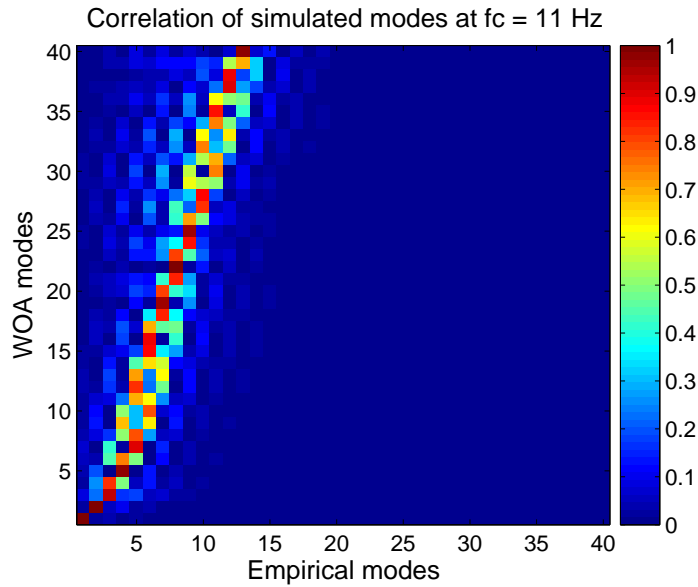


Figure 3.4: An image plot showing the correlation between the empirical modes and the ideal (input in this case) modes, where a 0 scale means they are not correlated and 1 means they are perfectly correlated. The simulation is created using the SVLA.

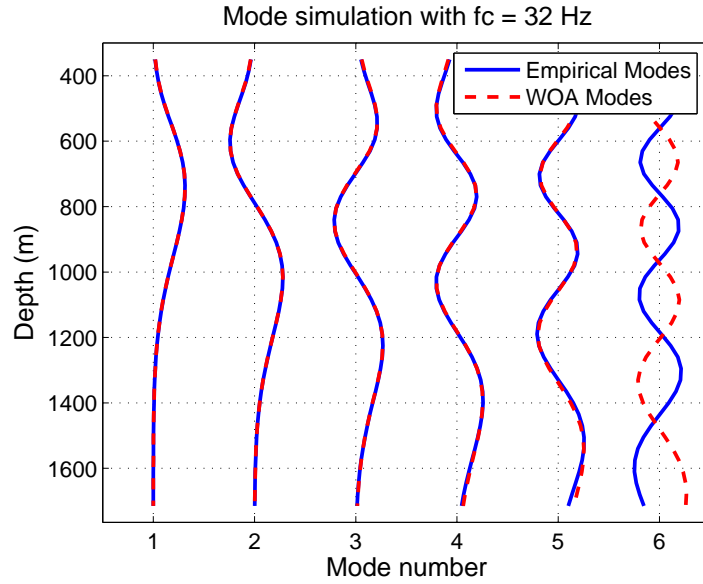


Figure 3.5: The extracted modes in solid blue lines and the input narrowband WOA modes at 32 Hz in red dashed lines. The simulation is created using the SVLA.

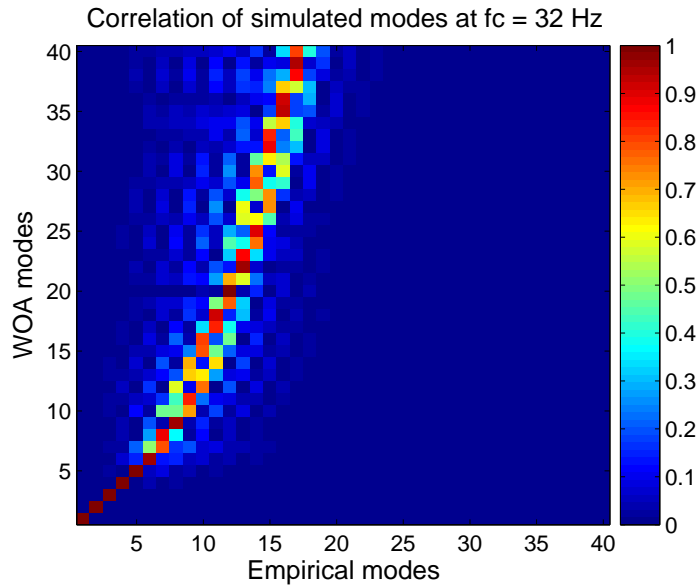


Figure 3.6: An image plot showing the correlation between the empirical modes and the ideal (input in this case) modes, where a 0 scale means they are not correlated and 1 means they are perfectly correlated. The simulation is created using the SVLA.

were at higher frequency there would be perfect correlation for more than the first 2 modeshapes. Figures 3.5 and 3.6 show the extracted modes and the correlation respectively in a simulation with a frequency of 32 Hz. From the figures it is evident that while still using the same array aperture it is possible to extract more modeshapes if the modes are propagating at higher frequencies.

3.3 Snapshot Problem

The previous two sections presented a model that generates the CSDM \mathbf{R} in one step. In a more practical environment multiple receptions (snapshots) have to be averaged over time to generate a good estimate of the CSDM. Typically, in array processing, the minimum requirement for generating a good estimate of the matrix \mathbf{R} has to be $K \geq 2N$ snapshots (according to Reed *et al.* [16]), where N is the number of receivers. This section discusses how the number of snapshots impacts the ability to estimate the modeshapes from noise data in simulations using the eigendecomposition of the CSDM.

The k^{th} snapshot of the pressure field is generated by using:

$$\mathbf{p}_k = \mathbf{\Phi} \mathbf{a}_k , \quad (3.4)$$

where the matrix $\mathbf{\Phi}$ is a column matrix of the narrowband modeshapes and its dimensionality is (N by M), and the vector \mathbf{a}_k is the weighting vector for each mode and with dimensions (M by 1), where N and M are the number of receivers and the number of modes respectively. This makes the pressure field of size (N by 1). For simplicity the weighting vector \mathbf{a}_k is assumed to be random noise. A simple example is to make \mathbf{a}_k a complex Gaussian noise with zero mean and covariance matrix with diagonal elements 20% different from the adjacent elements.

Then the estimated CSDM $\hat{\mathbf{R}}$ is generated from the pressure field measurements by using the term in equation 3.4. Since the pressure field is narrowband then the matrix $\hat{\mathbf{R}}$ is generated by the outer product of the pressure \mathbf{p} as shown in the equation below

$$\hat{\mathbf{R}} = \frac{1}{K} \sum_{k=1}^K \mathbf{p}_k \mathbf{p}_k^H, \quad (3.5)$$

where K is the number of snapshots. Then the modeshapes can be extracted from the estimated CSDM by computing the eigendecomposition of $\hat{\mathbf{R}}$. The empirical modeshapes $\hat{\Phi}$ are equal to the eigenvectors of $\hat{\mathbf{R}}$.

There will be two parts of the simulation, the first one uses an array that spans the complete water column (*i.e.*, 1 m to 5000 m) for 2N, 50N and 100N snapshots. The second simulation is of an array that has the same aperture as the SVLA used in the previous section (spans depths from 350 to 1715 with 35 m spacing), also for 2N, 50N and 100N snapshots.

Figure 3.7 shows the first part of the simulation, when the array spans depths from 1 m to 5000 m with 35 m spacing between elements. The left column of the figure shows the modeshapes of the first 6 modes and the right column of the figure shows the correlation between the empirical modes and the WOA modes, *i.e.*, input modes to the simulation. The empirical modeshapes are shown in blue solid lines and the WOA modeshapes are shown in red dashed lines. The first, second, and third rows show the results of using 2N, 50N, and 100N snapshots respectively. It is evident from the plots that as the number of snapshots increases, the correlation between the extracted modeshapes and the true modeshapes improves. When 100N snapshots is used the estimate of the CSDM is consistent between every time it is simulated and the results are similar to the ones in section 3.1.

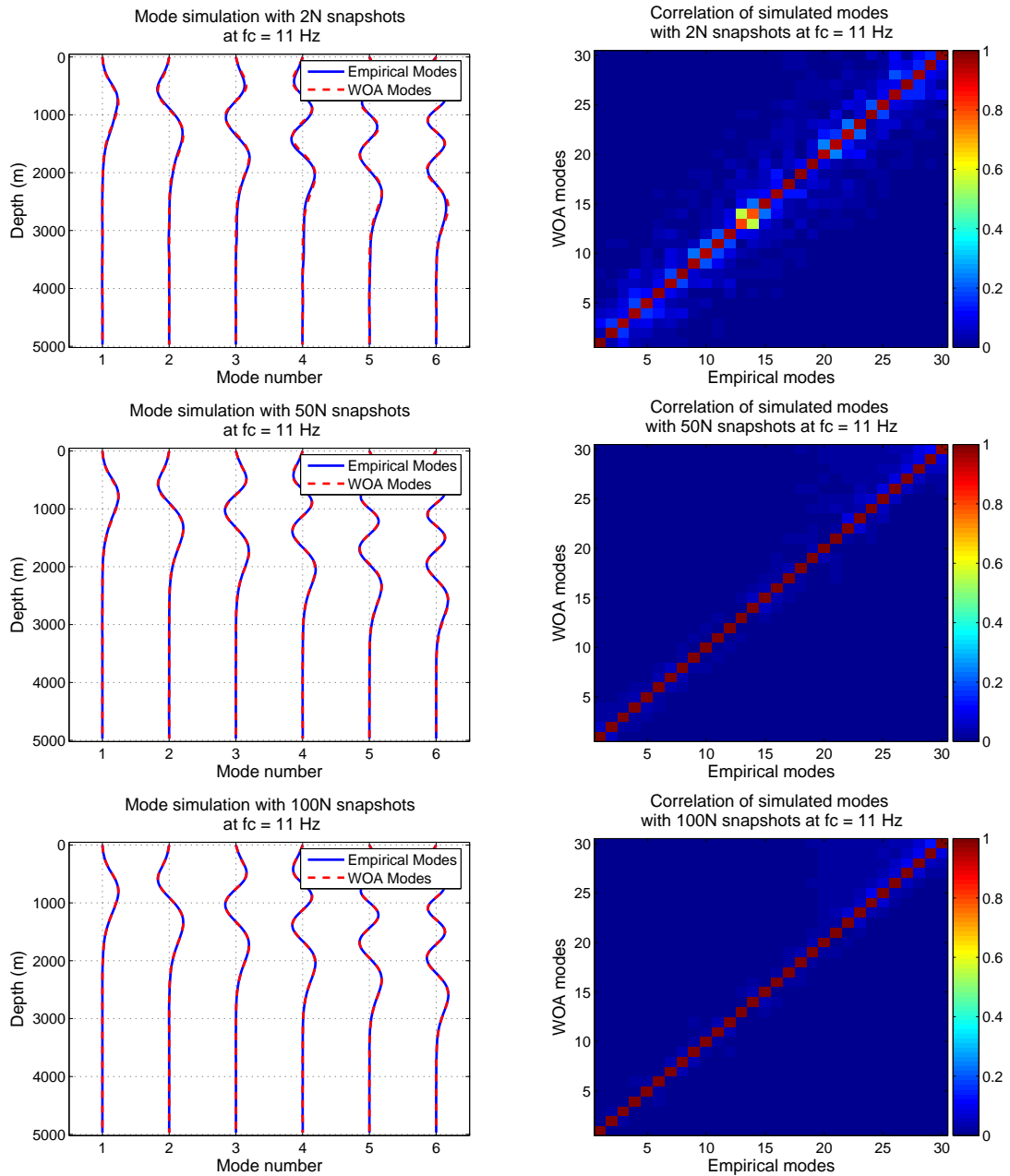


Figure 3.7: The effect of snapshots on modeshape extraction when using the water column spanning VLA. The left column shows the first 6 modeshapes, empirical modes shown in blue solid lines and the WOA modes shown in red dashed lines. The right column shows the correlation between empirical modeshapes and the WOA modes. The first row shows the results for 2N snapshots, the second row shows the results for 50N snapshots, and the third row shows the results for 100N snapshots.

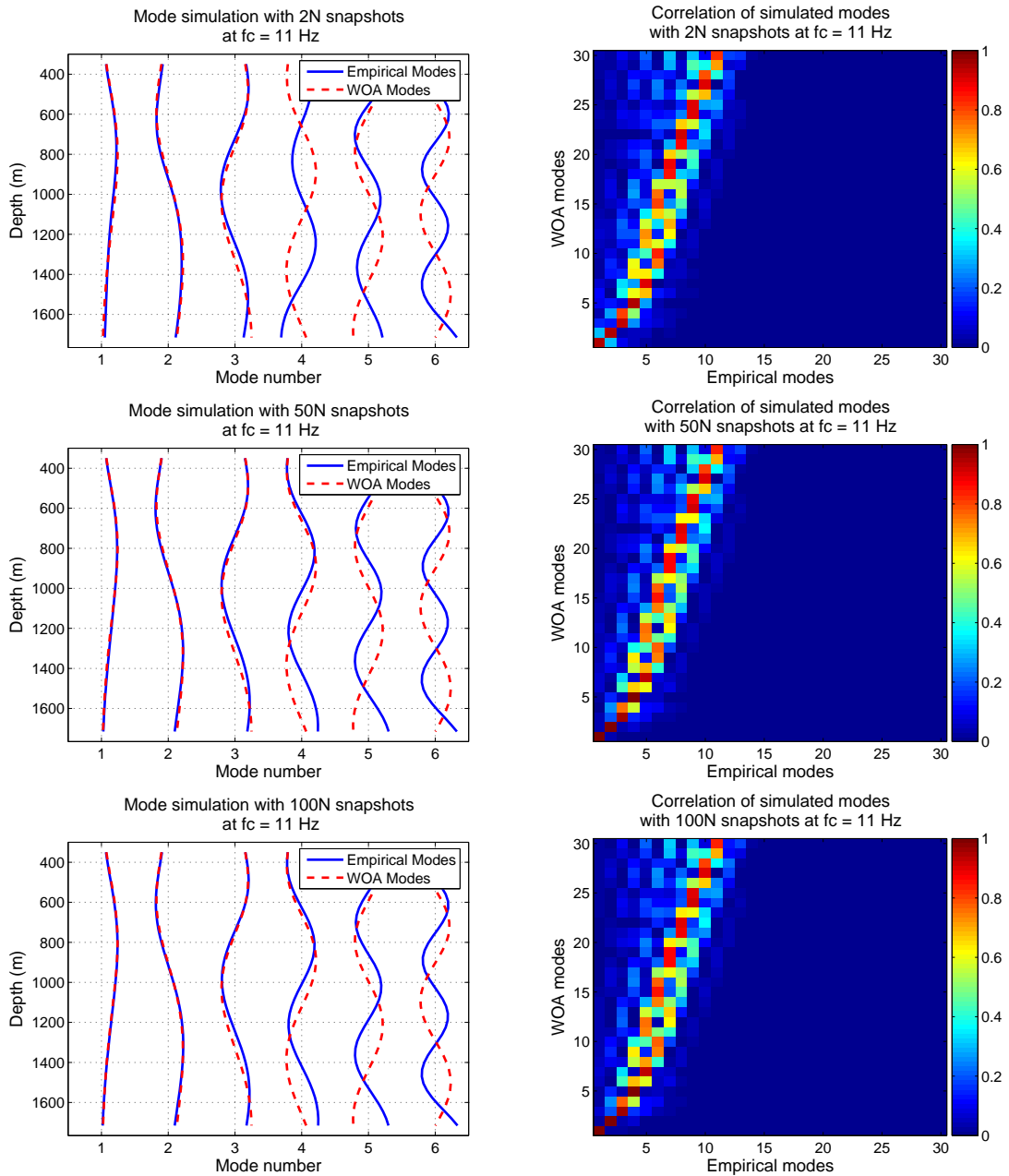


Figure 3.8: The effect of snapshots on modeshape extraction when using the SVLA. The left column shows the first 6 modeshapes, empirical modes shown in blue solid lines and the WOA modes shown in red dashed lines. The right column shows the correlation between empirical modeshapes and the WOA modes. The first row shows the results for 2N snapshots, the second row shows the results for 50N snapshots, and the third row shows the results for 100N snapshots.

The second part of the simulations for this section, shown in Figure 3.8, shows the simulation results for the SPICE04 SVLA. The left column of the figure shows the modeshapes of the first 6 modes and on the right column of the figure the correlation is shown between the empirical modes and the WOA modes (*i.e.*, input modes to the simulation). The empirical modeshapes are shown in blue solid lines and the WOA modeshapes are shown in red dashed line. The first, second, and third rows show the results of using 2N, 50N, and 100N snapshots respectively. The shorter array as seen in the figure is not as sensitive to the number of snapshots as the longer one, but it is still evident that when the number of snapshots is small the results change during every simulation, *i.e.*, the results are different every time the simulations are computed using the same number of snapshots in the simulations. When there are 100N snapshots the simulation results are consistent. Since 100N snapshots gave excellent results in simulations, we will use 100N as a minimum number of snapshots for the real data analysis in Chapter 4.

3.4 Array Tilt

In typical deep water experiments a vertical array is anchored at the bottom of the ocean and held upright by a subsurface buoy. Since the buoy can drift, the array does not remain perfectly vertical. In making the simulations of the VLA, the first step is setting up the coordinate system correctly to simulate array tilt or correct for it. Figure 3.9 depicts the three dimensional Cartesian coordinate system (x, y, z) used for modeling the VLA in 3-D space, where z is the depth in meters, x and y are the displacements in the azimuthal direction in meters. The figure shows the coordinate system with the VLA presented in red, where the VLA is anchored at $(0,0,0)$ with a vertical tilt angle of θ with respect to the z -axis, and a horizontal displacement angle

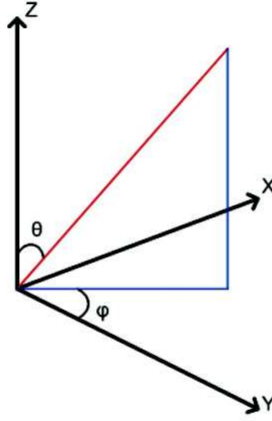


Figure 3.9: The VLA (red) anchored at the origin, with a vertical tilt angle θ , and a horizontal displacement angle φ .

of φ from the y -axis.

A closeup of the tilt of a VLA and how it is implemented in the same coordinates is presented in Figure 3.10. The dotted red line, in the figure, represents the original position of the VLA, the solid red line represents the current (*i.e.*, tilted) position of the array with each element a distance d to adjacent elements, Δz is the vertical displacement of each receiving element, and Δr is the distance of each element from the z -axis. The angle φ in the figure is assumed to be zero to simplify the simulations. The received pressure field when the array is perfectly vertical is not the same when the array is tilted. If the receiving array is assumed to be in the far field then the signals received are plane waves. In a tilted array the received signals will have a phase shift dependent on the displacement Δr of each receiver, where Δr is the change in range between the vertical axis and the receiver in the y direction. To simplify the implementation of shift on the signals made by each of the receivers, the shift is implemented as a phase shift of the received narrowband pressure field as shown in the equation below.

$$\mathbf{p}_{\text{tilt}} = e^{jk_1 \Delta r} \mathbf{p}, \quad (3.6)$$

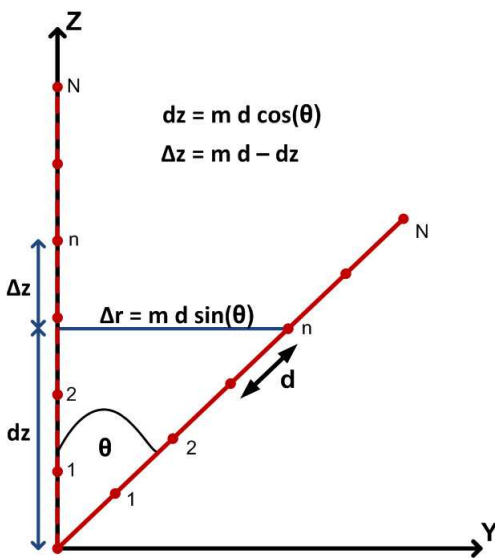


Figure 3.10: The tilted VLA (represented in a red solid line) with elements 1,2,...,N (red dots) with distance d between elements, and the vertical red dashed lines represent the original position of the VLA. Δr is the distance of each element from the z -axis, and Δz is the vertical displacement of each element.

where \mathbf{p}_{tilt} is the tilted version of received narrowband pressure field \mathbf{p} , and k_1 is the wavenumber (as shown in equation (2.3)) of the first mode. The wavenumber for the first mode is used because the distance Δr is assumed to be small relative to the depth of the water column, thus the change in phase due to different wave numbers is small at those small distances.

The change in depth changes the sample locations that the modeshapes are sampled at. This just means that the modeshapes, when the array is perfectly vertical, will look different than the modeshapes when the array is tilted and the sensors are displaced in depth due to the tilt. During the simulation the changes in depth are assumed to be known.

Since the water column spanning array is long (*i.e.*, 5000 m) as shown in Section 3.1, that array should be affected by tilt more than the SVLA. The reason is that at small tilt angles the displacement in x or Δr are large in the water column

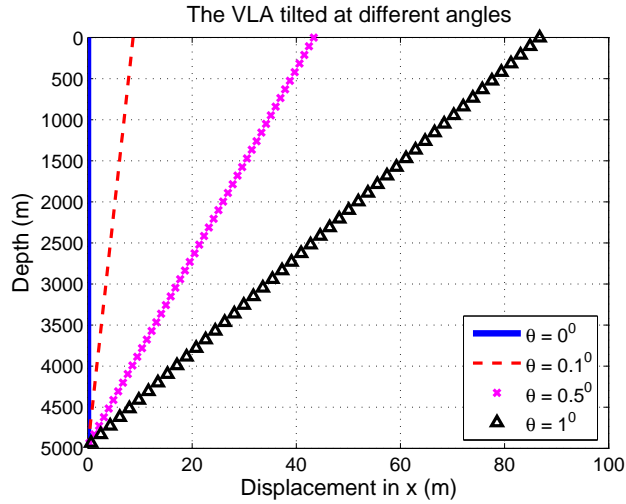


Figure 3.11: A plot showing the water column spanning array in deep water tilted at 0° , 0.1° , 0.5° , and 1° represented as a solid blue line, A dashed red line, magenta colored stars, and black triangles respectively.

spanning array relative to displacements in a tilted SVLA. In Figure 3.11 a plot of the tilted array at the different angles is shown. The solid blue line represents the perfectly vertical array, the red dashed line represents the array tilted by 0.1° degrees, magenta colored stars are for an array tilted by 0.5° degrees, and the black triangles represent the array tilted by 1° degree.

The plots in Figure 3.12 show the correlation and the first 6 modes at tilt angles 0° , 0.1° , 0.5° , and 1° . In the figure, the effects of tilt on the empirical modes is clear even for small increments of tilt angles. The displacement of the elements on the array in depth is very small. The horizontal displacements in the x direction from Figure 3.11 is larger, where the top hydrophone displaces from 0 m to about 87 m with respect to the bottom hydrophone with a tilt angle of 1° degree.

The same tilt angles are implemented on an array that has the same configurations as the SVLA in the SPICE04 experiment. Figure 3.13 shows the tilted array at the different tilt angles. The solid blue line represent the perfectly vertical array, the

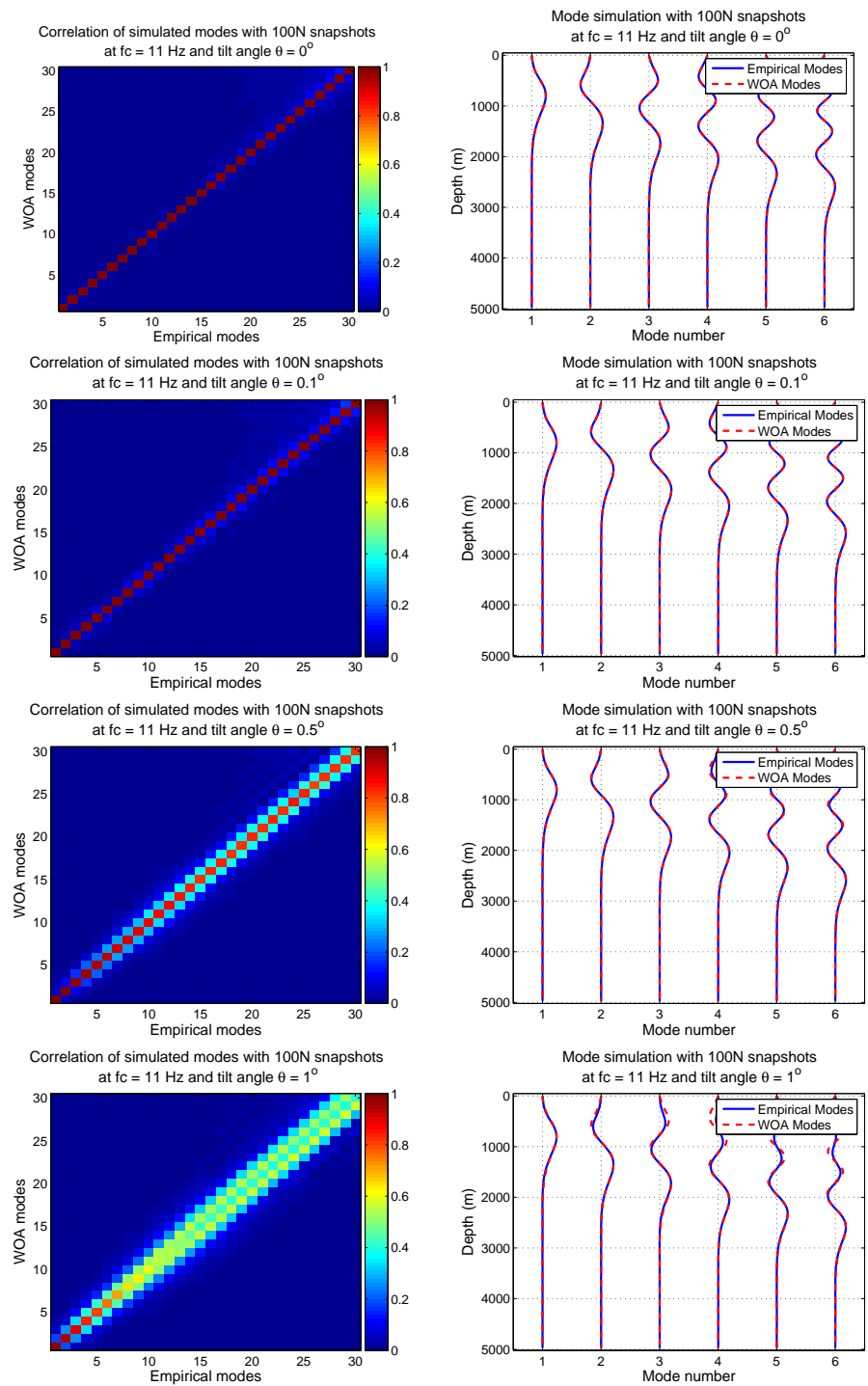


Figure 3.12: Correlation and modes shown for a VLA that spans depths from 1 m to 5000 m with a 35 m spacing, when the array is tilted at angles 0° , 0.1° , 0.5° , and 1° .

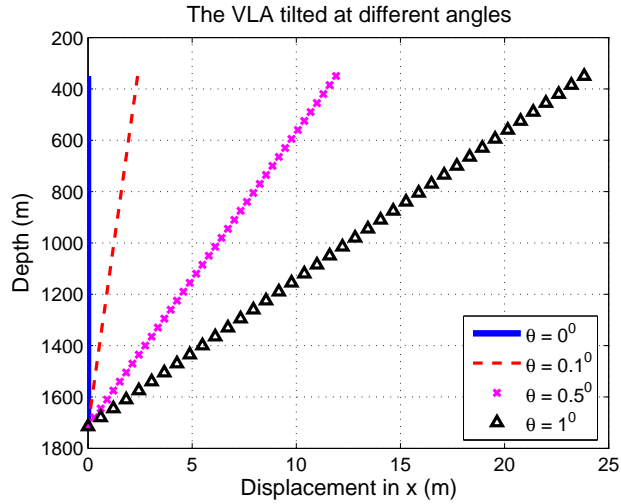


Figure 3.13: A plot showing the SVLA tilted at the different angles. A solid blue line represents the perfectly vertical array. A dashed red line when the array is tilted by 0.1° degrees, magenta colored stars for an array tilted by 0.5° degrees, and black triangles when the array is tilted by 1° degree. Note the different scale in the x -axis and the y -axis relative to Figure 3.11.

red dashed line represents the array tilted by 0.1° degrees, magenta colored stars are for an array tilted by 0.5° degrees, and the black triangles represent the array tilted by 1° degree. The figure shows the effect of the shorter array on the displacements of the receiving elements, where the changes in displacements is smaller from one tilt angle to another compared to the longer array.

The plots on Figure 3.14 show the correlation and the first 6 modes of the array tilted with angles 0° , 0.1° , 0.5° , and 1° . The results from the plots in Figure 3.14 are much better than in Figure 3.12. The array used to generate the plots in Figure 3.14 is much shorter, which makes the array less sensitive to small changes in the modeshapes. The array does not span the depth of some of the modes, which is the main reason the array is not as sensitive as a longer array, where the array can detect small changes in the complete modeshape rather than a part of the modeshape.

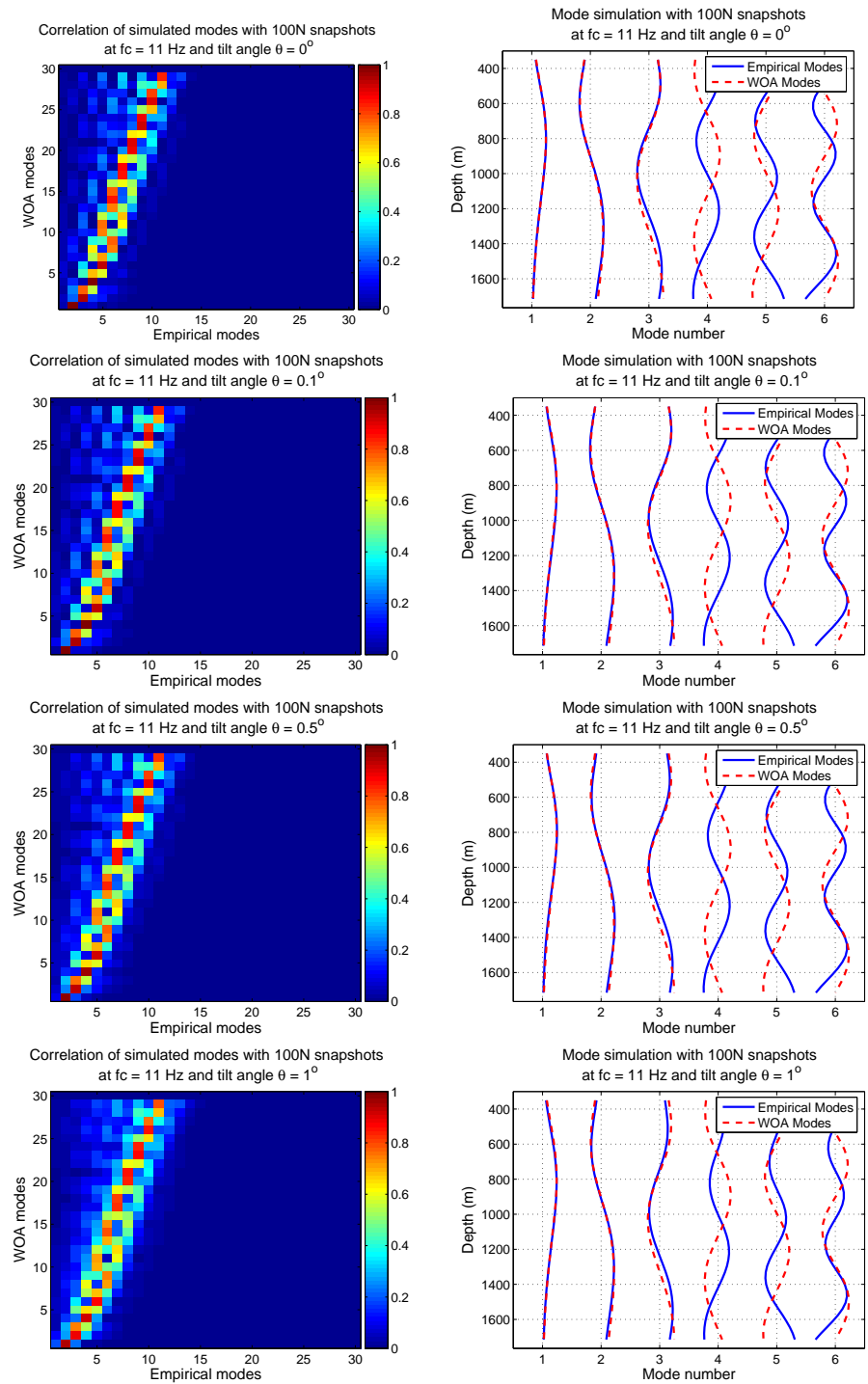


Figure 3.14: Correlation and modes shown for a VLA that spans depths from 350 m to 1750 m with a 35 m spacing, and tilted at angles 0° , 0.1° , 0.5° , and 1° .

3.5 Filter Design

The filter design is critical for extracting modeshapes in this thesis, because the modes are frequency dependent. The size of the filter used to process the received pressure field measurements affects the number of snapshots available for computing the CSDM \mathbf{R} . The longer the filter in time, the fewer independent snapshots used to compute the matrix \mathbf{R} . Using a shorter filter provides a wider filter bandwidth in the frequency domain, which may not yield accurate extraction of modeshapes due to the fact the mode functions are frequency dependent.

The modeshapes change only a little across a band of frequencies, therefore a filter that passes only one frequency is not necessary for this application. If the modeshapes are unchanged across a band of frequencies, then the filter can have a relatively wider bandwidth. The correlation is calculated by using the equation below.

$$S_{corr} = \phi_{f_c}^H \phi_{\Delta f} , \quad (3.7)$$

where the correlation between the shapes in frequency S_{corr} is the inner product between the modeshape ϕ_{f_c} at the desired center frequency and the modeshapes $\phi_{\Delta f}$ in the frequency range $f_c \pm 10$ Hz .

Figure 3.15 shows the correlation of the WOA mode 1 and mode 10 with themselves at center frequencies of 10 Hz, 20 Hz, 30 Hz, and 40 Hz to show how correlated they are across frequency for the VLAs discussed in sections 3.1 and 3.2. The blue solid lines represent the modes created if the SVLA had the same properties as the VLA used in the SPICE04 experiment, where the array consisted of 40 elements that spanned depths from 350 m to 1715 m with 35 m spacing between elements. The red dashed line represents an ‘ideal’ array, one that spans the water column consisting of 5000 elements and sampled depths from 1 m to 5000 m with 35 m spacing between

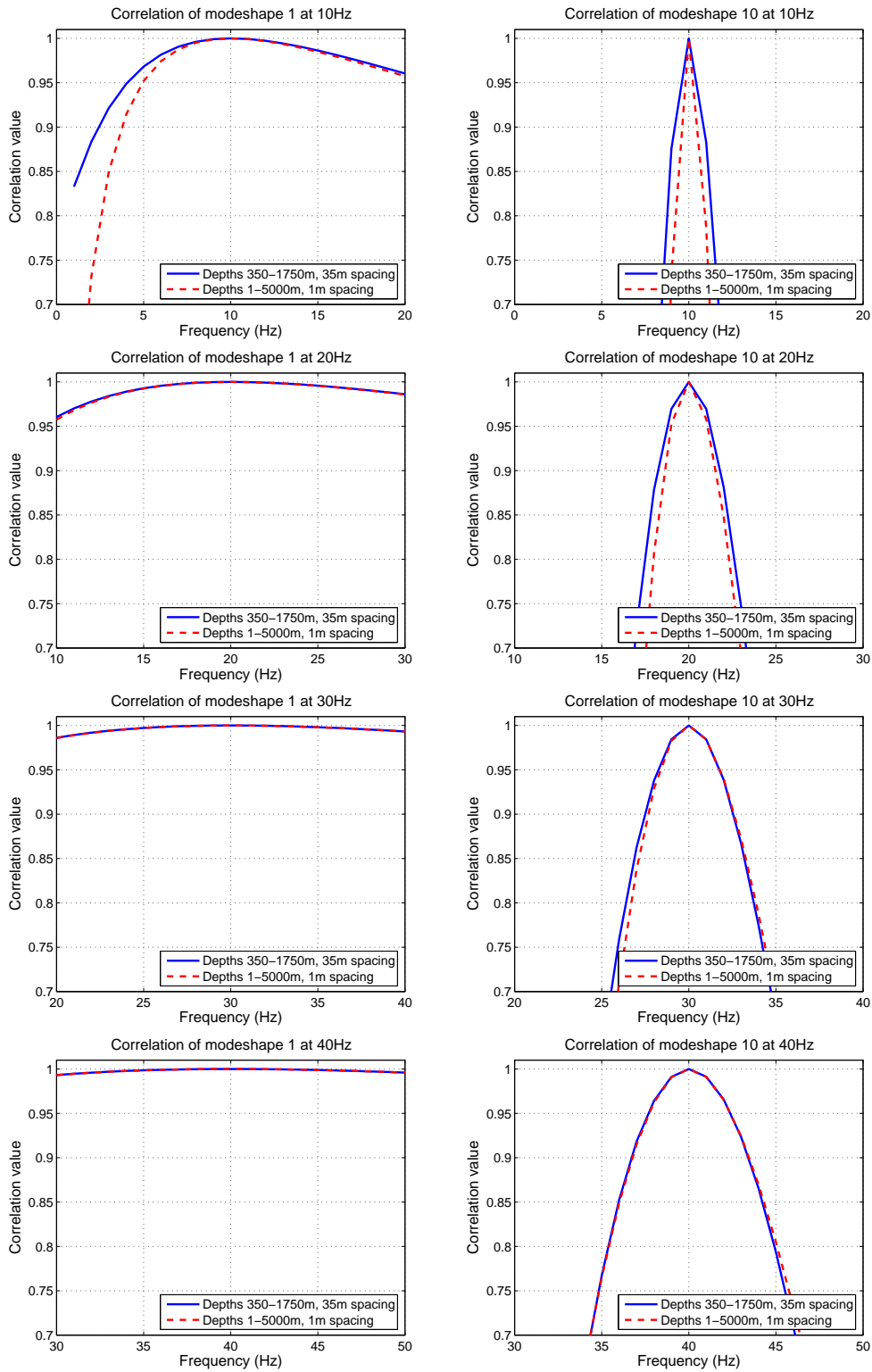


Figure 3.15: Plots of the correlations of modes 1 and 10 with themselves across frequency, which is used to aid filter design.

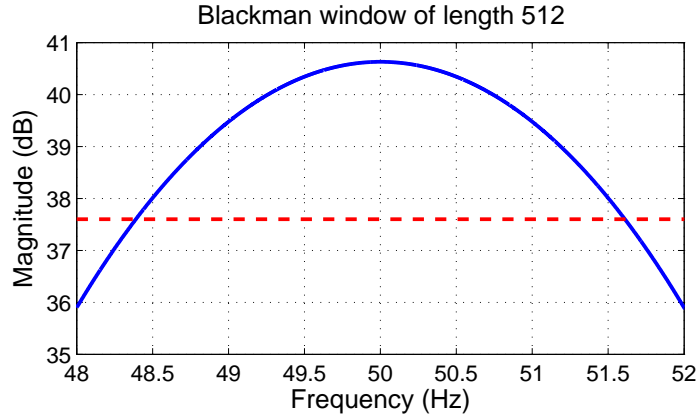


Figure 3.16: A plot showing the Magnitude and the Phase of the Fourier transform of the Blackman window with a center frequency of 50 Hz. The red dashed horizontal line indicates the 3dB down mark.

elements. The plots clearly show that as the frequency increases the correlation for mode 10 and for mode 1 is higher across about a 3 Hz bandwidth. From the plots in the figure the ‘ideal’ array seems to be doing worse than the set up of the VLA used in the SPICE04 experiment (in blue solid curve), but in fact it is doing better in the sense that it is more sensitive to small changes in frequency for modes 1 and 10. The reason is that as the VLA used in SPICE04 may not span the depths of the modes, which makes it less sensitive to changes in the regions that the array does not sample.

The filter used to process the receptions of the ambient noise pressure field needs to have linear phase and good sidelobe attenuation. Throughout this thesis a Blackman filter is used to filter the pressure field measurements. The Blackman filter is very simple to design and has excellent sidelobe attenuation, where the peak sidelobe amplitude relative to the mainlobe is -57dB [17].

From the plots in Figure 3.15 there is enough correlation that it is possible to use a Blackman window that has 3 Hz bandwidth at 3dB down (*i.e.*, $f_c \pm 2$). Figure 3.16 shows the magnitude plot of the filter used throughout this thesis, which is a 512 point length filter in the time domain. The plot shown in the figure is centered

at 50 Hz, and the red dashed horizontal line represents the 3dB down mark.

3.6 Summary

The narrowband pressure field in this chapter is simulated using narrowband modeshapes and the technique of extracting the modes using eigendecomposition is studied in different simulations. The modes can be extracted if the measurements of the pressure field are taken using a VLA. The first section in the chapter proved that it is possible to extract the modes by calculating the eigenvalues of the CSDM, when a VLA is used to sample the pressure field at all depths of the water column. The second section presented simulations using a shorter array, specifically the SVLA used in the SPICE04 experiment. The results from simulating an array that was short (compared to the water column) and centered around the axis of the acoustic channel (*i.e.*, minimum of the SSP) showed that it is possible to extract at least the first couple of modes. The number of snapshots needed to compute a good estimate of the CSDM is shown to be around $100N$ snapshots. That number of snapshots was the minimum that generated consistently good modeshapes that were similar to the modeshapes extracted from the narrowband model presented in sections 3.1 and 3.2. The last section showed the effect of array tilt on the extracted modeshapes, where the effect on the extracted modes is larger when the array spans the complete water column. The extracted modeshapes from the VLA used in the SPICE04 experiment were not affected a lot by small angles due to its size.

From the results of this chapter, a good estimate of the modeshapes can only be achieved if the following criteria is met. (1)The VLA must span the complete water column in order to extract N modeshapes. If the array does not span the complete water column then only some of the low order modes can be extracted. (2)Extensive

sampling of the water column is important for mode extraction.

The filter design is crucial to the extraction of modes, because it essentially affects the number of snapshots needed. Ideally a really narrowband filter, that passes only one frequency, would be used, but that would make the filter long in time and therefore the number of snapshots is less. From the plots in Figure 3.15 of the modeshape correlation across frequency for several frequencies, the modes are correlated in roughly a 3 Hz bandwidth. A filter of roughly a 3 Hz bandwidth is designed to filter the received pressure field in the next chapter. The filter has the shortest time window possible, such that when it is used on the data there would be a sufficient number of snapshots, at least $100N$, required to compute a good estimate of the CSDM \mathbf{R} . The exact number of snapshots used to calculate \mathbf{R} from the SPICE04 receptions is presented in the next chapter.

Chapter 4: Experimental Results (SPICE04)

The previous chapter discussed and analyzed simulation results. This chapter discusses the experimental results of estimating modes from ambient noise measurements made during the SPICE04 experiment. A brief overview of the SPICE04 experiment is given in section 4.1. The setup of the VLA in the SPICE04 experiment is discussed in section 4.2. Section 4.3 describes an analysis of the noise measurements made during the SPICE04 experiment. Section 4.4 presents the results of extracting the modes from ambient noise data recorded during the SPICE04 experiment. The last section summarizes the chapter.

4.1 SPICE04 overview

The SPICE04 experiment was a part of a larger project conducted by the North Pacific Acoustic Laboratory (NPAL) group. There were several different experiments being conducted with multiple transmitters and receivers. The transmissions and receptions for the SPICE04 experiment officially began in June 2004, which was when the receivers and transmitters were deployed. The receiving line arrays and the transmitters were recovered about 12 months later in June 2005. The receptions are labeled in yeardays, where yearday 1 refers to the first day of the year the experiment started, which would be 2004 in this experiment. The parts that make the SPICE04 experiment consisted of 3 transmitters and 2 receiving arrays.

On the transmitting side there were three sources at different locations, which are S1, S2, and a source placed near Kauai. Sources S1 and S2 were transmitting

acoustic signals with a center frequency of 250 Hz. The sources worked for about 6 months and then they stopped transmitting signals due to hardware problems, which resulted in a large ambient noise data set being recorded by the VLA's.

The receiving end of the SPICE04 experiment consisted of two vertical arrays a Shallow Vertical Line Array (SVLA) and a Deep Vertical Line Array (DVLA). The SVLA and DVLA were not recording continuously when they were deployed, but were programmed to record periodically when a source is transmitting. When the sources S1 and S2 stopped working the VLAs continued to record at the times there was presumably a signal present. This provides about 6 months worth of ambient noise measurements to be analyzed. The receiving array was sampling the receptions at a sampling frequency $f_s = 4f_c = 4 \cdot 250 = 1000$ Hz. Only the SVLA ambient noise receptions during the receive windows for S1 and S2 are analyzed in this thesis. A map showing the SVLA/DVLA locations, and the location of the three sources in the north Pacific ocean is shown in Figure 4.1, where the SVLA/DVLA are shown as a red dot, and the sources as white triangles.

4.2 SPICE04 SVLA setup

Section 4.2.1 describes the physical setup of the receiving VLA, *i.e.*, the SVLA, used in the SPICE04 experiment. A detailed description about the periods the VLAs were recording and how the data was analyzed is discussed in section 4.2.2.

4.2.1 Setup

On the receiving end there were two receiving arrays as mentioned in the previous section. Only the SVLA is studied in this thesis. The SVLA had 40 hydrophone

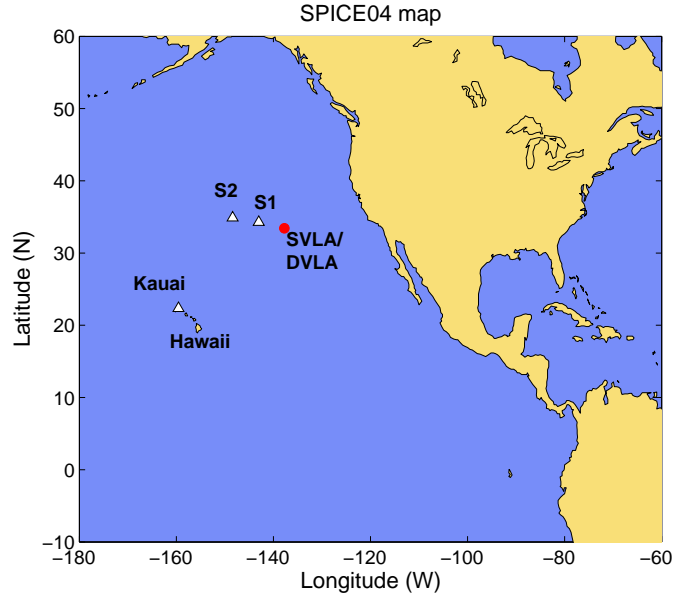


Figure 4.1: A color map showing the location of the SVLA/DVLA in the north Pacific ocean represented as a red dot, and the sources S1, S2, and the Kauai as red triangles.

elements spanning depths from 350 m to 1715 m with a 35 m spacing between elements, and was deployed in a 5000 m of water. In Figure 4.2 the position of the receiving elements are shown in the same plot as the SSP. Note that the depths of the hydrophones were chosen to sample the water column around the acoustic channel.

Figure 4.3 shows a rough sketch of the SVLA in a 3-D coordinate system. The red dots represent the locations of the 40 receiving hydrophones that have a spacing of 35 m between each element. The 40 hydrophones were divided into 2 parts. Each set of 20 hydrophones was connected to an AVATOC data acquisition system, where all the data in the array is processed. The AVATOC units applied front-end filtering to the receptions and then stored the data. They also stored the navigation data (*i.e.*, the navigation pings) of the SVLA. The location of the hydrophones was determined using the method of triangulation using a set of 4 acoustic transponders (shown as purple triangles in Figure 4.3) placed at the bottom of the ocean floor and acoustic

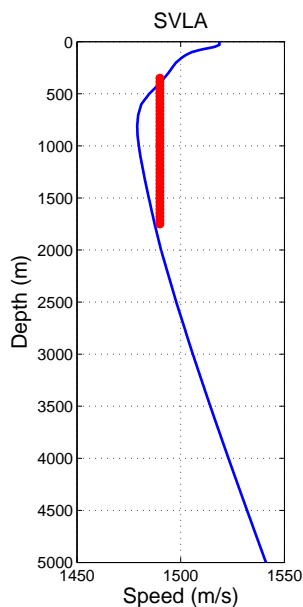


Figure 4.2: A plot showing the positions of the receiving elements in depth (shown as red dots) relative to the SSP (in solid blue line) from the WOA database [2].

transponders located on the receiving array.

Throughout the experiment temperature, pressure, and salinity sensors on the array sampled the environment. The sensors have been recording data every 5 to 7 minutes making available a large data set of the ocean parameters throughout the experiment. The parameters make it possible to compute the actual SSP at that location for any time during the experiment.

4.2.2 Receptions

The recordings made by the receiving elements in the SVLA were set up such that each recorded file corresponds to a source S1 or S2. The sampling frequency, as stated in the previous section, for the receptions in the SPICE04 is at a frequency of 1 kHz. The recordings of the ambient noise measurements (*i.e.*, the times that

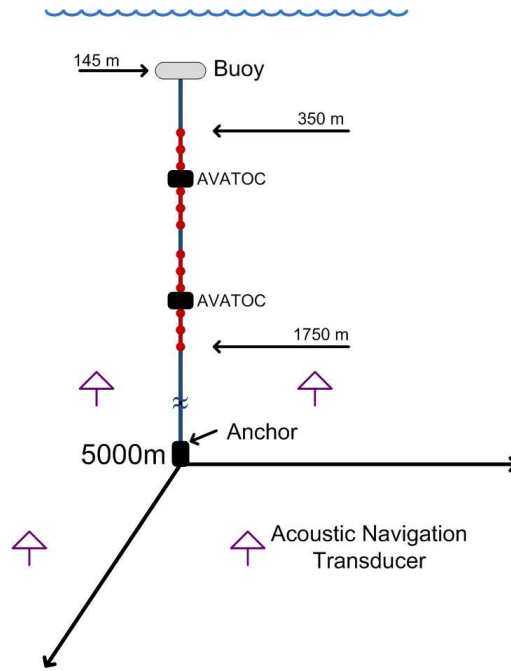


Figure 4.3: A rough 3 dimensional image of the Shallow Vertical Line Array (SVLA) used in the SPICE04 experiment. The red dots represent the receiving hydrophones.

were set for the S1 and S2 receptions) are made 6 times a day on the 00, 04, 08, 12, 16, 20 hours, in a 24-hour clock. During each hour there are 4 measurements made starting at the 35:42, 41:20, 45:26, 51:03 (minutes:seconds) minutes relative to each hour. The 35th and 41st minute segments are 122.76 seconds (or 122760 samples or snapshots) long, and the 45th and 51st minute segments are 155.4960 seconds (or 155496 samples or snapshots) long. In total there are about 48 files per day, because there are 2 files for every reception segment, the first file contains the recordings of the top 20 elements of the array and the second file contains receptions from the bottom 20 elements. During every hour of receptions, it is possible to combine the 4 different receptions made in the, roughly 17 minute, overall interval in that hour. The reason those files are combined is because we are assuming that the ocean's ambient noise does not vary much during that time.



Figure 4.4: Block diagram showing the preprocessing steps implemented on the received pressure field to extract the normal modeshapes.

After analyzing the receptions from all hydrophones, there are 5 hydrophones with bad receptions. The ‘bad’ receptions means that the receptions made by those hydrophones is not consistent with the other hydrophones. The remaining good hydrophones, from top to bottom, are hydrophones 1 to 33, 38 and 39.

4.2.3 Preprocessing

Several preprocessing steps are required prior to extracting the modes from the data. The steps are to combine the top and bottom files, subtract off the mean from the receptions, implement the clock corrections between the top and bottom sets of receivers, and narrowband filter the received pressure field. Figure 4.4 shows the required preprocessing steps.

On the array each AVATOC data acquisition system is connected to 10 elements above it and another 10 elements below it. The reason is that each AVATOC system can manage only 20 receiving elements over the period the SVLA was deployed. Since the top 20 hydrophones and the bottom 20 hydrophones are connected to separate AVATOC data acquisition systems, the time that the receptions are written on the hard drives is not the same for each AVATOC. During the course of the experiment the two AVATOC systems were linked together to check and record clock drift between the upper and bottom halves of the array. The recorded files between the top and bottom halves of the array need to be shifted appropriately in time to properly align the receptions. The clock corrections are implemented in the frequency

domain for simplicity. This is done by simply finding the shift in the time domain then multiplying the Fourier transform of the signal by the term $e^{j\omega t_c}$, where t_c is the desired clock correction.

Because the modes are frequency dependent, the receptions must be narrow-band filtered prior to mode processing. The pressure field is also filtered by multiplication of the Fourier transform of the filter with the Fourier transform of the received pressure field, which is not as computationally intensive as convolution is in the time domain. For computational efficiency the received pressure field is shifted (clock correction) and filtered at the same time, as implemented in the second block in Figure 4.4.

4.3 SPICE04 Noise

This section presents an analysis of ambient noise statistics. In order to understand the underwater noise receptions, the Power Spectral Density (PSD) is computed of the noise receptions over time. The PSD shows where the power is concentrated in frequency. This allows us to compare how the power varies from day to day during the SPICE04 experiment. The PSD is computed using the standard Welch-Bartlett method with a 2048 point Hamming window with 50% overlap [17].

Figure 4.5 shows scaled image plots of the PSD of the noise over time, for the top hydrophone (depth $\simeq 350$ m), the middle hydrophone (depth $\simeq 1015$ m), and the bottom working hydrophone (depth $\simeq 1680$ m). As the figure shows, most of the power lies in the bandwidth from about 10 Hz to 90 Hz. Looking closely at the plot of the PSD from the measurements made by hydrophone 1, there are some very low frequency components with significantly higher power than in other frequencies and in the PSD plots of other depths. These spikes in low frequencies are present on some

of the yeardays during the SPICE04 experiment. The reason for those low frequency components is not completely clear, but could have been caused by a storm at the surface over the SVLA or high windstress during those yeardays.

The average PSD measurements of the ambient noise over time of receptions from hydrophones 1, 20 and 39 are shown in Figure 4.6. In the PSD of the receptions from hydrophone 1, the low frequency components have significantly higher power than other frequency components. The low frequency components, from the averaged plot of the PSD from measurements made by hydrophone 1, lie around 3 Hz to about 20 Hz with a max at 11 Hz with power of about 16dB higher than the maximum value in the averaged plots of the PSD from hydrophones 20 and 39. For hydrophones 20 and 39 the PSD rolls off towards low frequencies due to input filters implemented on the data as they are received.

4.4 Noise Modeshapes

In this section the method discussed in Chapter 2 is implemented to extract the modeshapes from the ambient noise receptions. This section is split into two subsections, because we have noticed that during some yeardays the extraction of the modes looked similar to some of the results from the simulations, and during some yeardays the shapes of the eigenvectors of the CSDM did not look like modeshapes. Section 4.4.1 presents the approach to extracting the modes and some results, where the extracted modeshapes looked like the actual modeshapes. Section 4.4.2 presents the results of data from yeardays where the extraction was not successful.

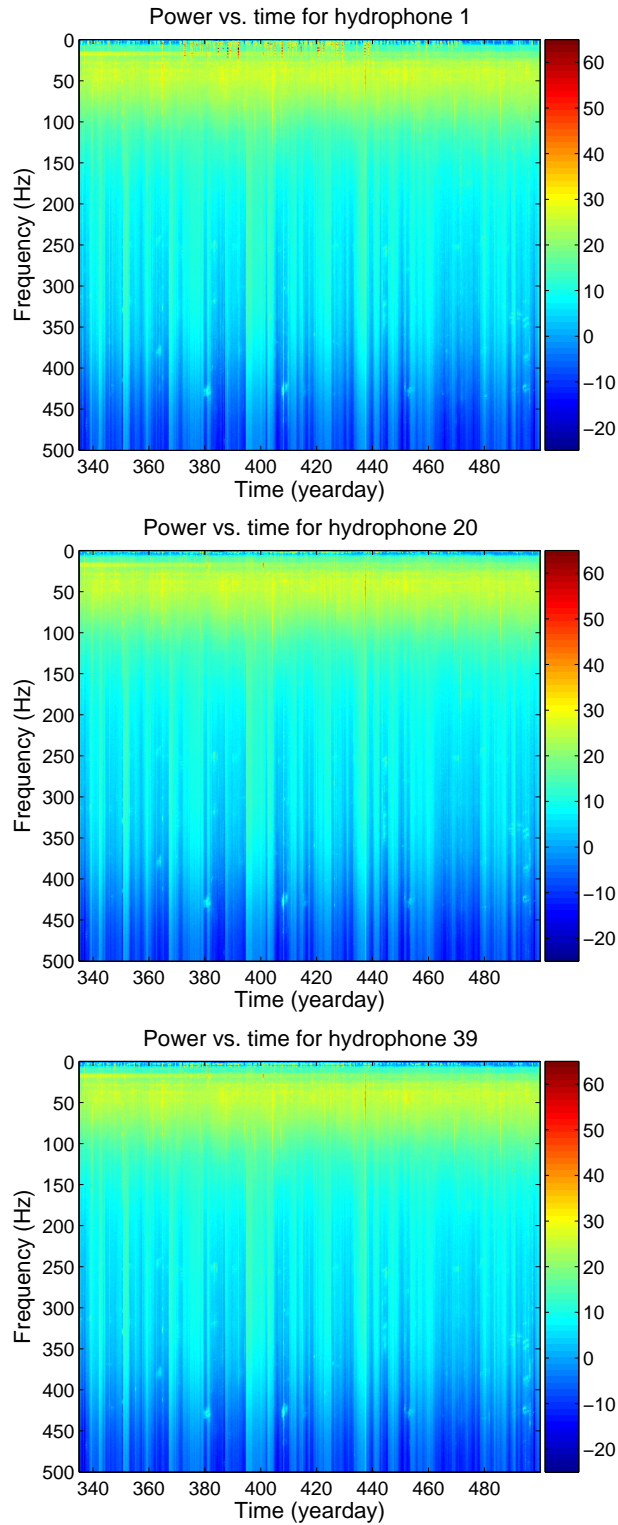


Figure 4.5: Plots of the Power Spectral Density (PSD) of the ambient noise receptions over time at hydrophones 1, 20 and 39, which are at a depths of about 350 m, 1015 m, and 1715 m, respectively.

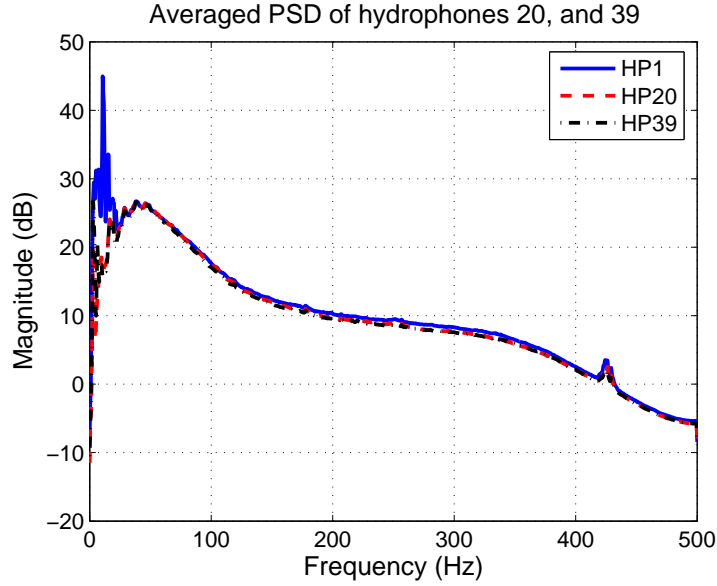


Figure 4.6: Plot showing the averaged Power Spectral Density (PSD) over time of the ambient noise receptions at hydrophones 1 (shown in a solid blue line), 20 (shown in a dashed red line), and 39 (shown in a black dash-dotted line), which are at depths of about 350 m, 1015 m, and 1715 m respectively.

4.4.1 Good Extraction

The number of snapshots used is very crucial for constructing the CSDM \mathbf{R} , which depends on the size of the filter used. In section 3.3 of the previous chapter the best filter length for this application is found to be a 512 point length filter. If 4 receptions are combined on a yearday during an hour then the number of snapshots present using this filter would be about 2176 snapshots per hydrophone with 50% overlap, which means we have $(2176/35) N \cong 725N$ snapshots to generate the CSDM \mathbf{R} .

Because the modes are frequency dependent, the first step for computing the modes is to find a center frequency for the filter to extract that frequency from the pressure field measurements. Figure 4.7 shows a zoomed in version of the averaged PSD from Figure 4.6 of only hydrophones 20 and 39. From the figure most of the power is concentrated around 37 Hz.

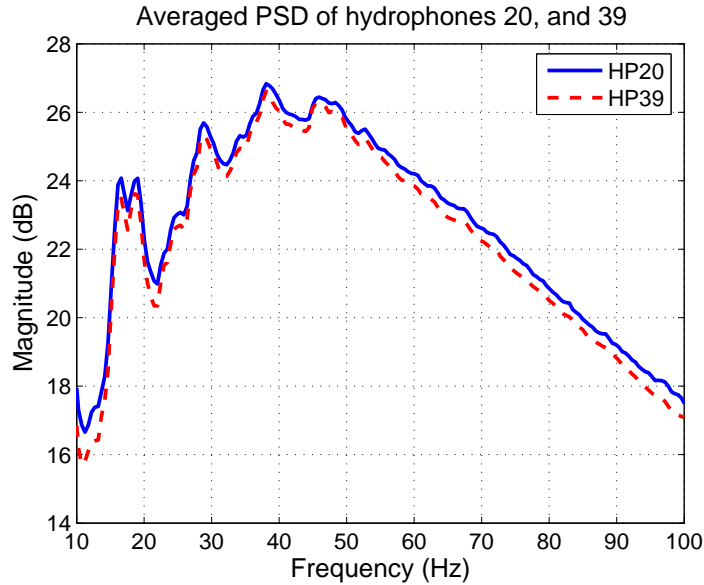


Figure 4.7: A zoomed in version of Figure 4.6 of the averaged ambient noise receptions over time at hydrophones 20 and 39, which are at a depths of about 1015 m and 1715 m respectively.

Using the same filter discussed in chapter 3, a single modeshape is extracted at center frequencies 8 Hz to 44 Hz with 3 Hz increments because of the bandwidth of the filter. Figure 4.8 shows the extracted modes 1, 2, 3, and 5 in solid blue lines from measurements made on yearday 455. The extracted modes are compared to the actual modes at that yearday, calculated from the measured environmental data, in the dashed red lines. The extracted modeshapes for mode 1 at 11 Hz, 14 Hz, and 17 Hz look like they have the same modeshape as the actual modes. The same can be said for mode 2 at the same frequencies. The extracted modeshapes for modes 3 and 5 do not have the same modeshapes as the actual modes, but they also look like they are getting better as we go up in frequency. The modeshapes for modes 3 and 5 even at higher frequency span more depths than the array is sampling, therefore they will not be the same as the actual modes. It is evident from the plots that the extracted modes at a lower center frequency look better only for the first couple of modes. The center frequency of 11 Hz is chosen through out the thesis because the

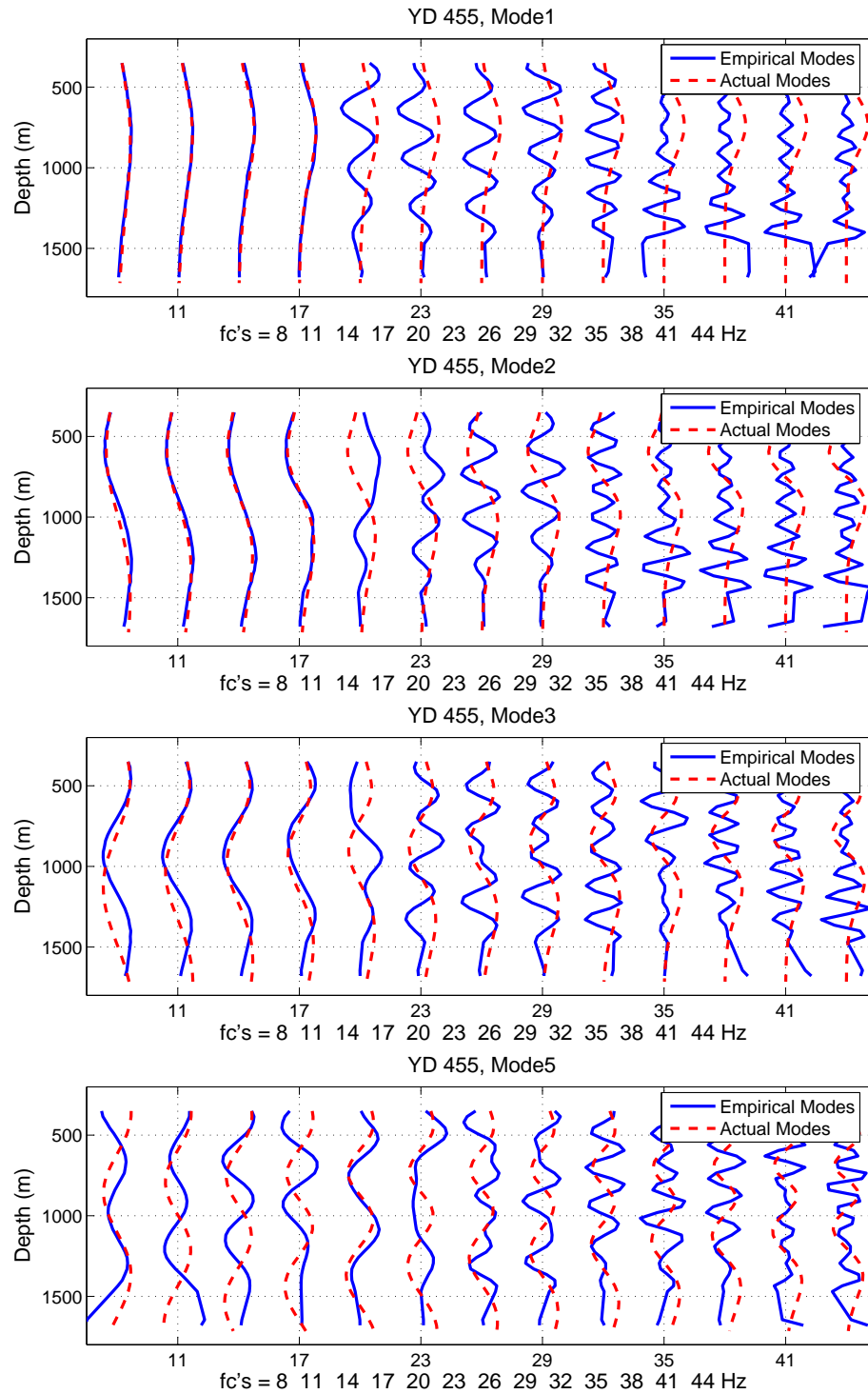


Figure 4.8: The extracted modeshapes of modes 1, 2, 3, and 5 on yearday 455 (shown in blue solid lines) compared to the actual modeshapes from the measured SSP (shown in red dashed line). The modes are plotted for center frequencies 8 Hz to 44 Hz with 3 Hz spacing between frequencies due to the bandwidth of the filter.

empirical modeshape 2 is smoother at that frequency than 14 Hz and 17 Hz.

Using the correlation method discussed in chapter 3, the modes at 11 Hz are compared for several yeardays in Figures 4.9, and 4.10. The first 9 empirical modeshapes are shown in solid blue lines and the actual modeshapes are shown in red dashed lines in the plots on the left. The right plots in the figure are the correlation plots of the modeshapes between the empirical modes and the actual calculated modes. Figure 4.9 shows the modes for yeardays 347 and 401, and Figure 4.10 shows the modes on yeardays 455 and 491.

The modeshapes shown in Figures 4.9 and 4.10 are for yeardays that are considered yeardays with good receptions, where the received pressure field measurements provide very good modeshapes. There are some yearday receptions (about 30 yeardays or roughly 180 receptions) where the shapes of the extracted vectors do not look like modeshapes.

4.4.2 Bad Extraction

The eigendecomposition method introduced Chapter 3 assumes that the sources are far enough such that the received modes are independent. If there is a storm or high windstress directly above the array, then the source is close to the array. When the source is close to the array the eigendecomposition method cannot be used to extract the modeshapes.

Figure 4.11 the empirical modeshapes for some of the yeardays, where the shapes did not look like modes, the first nine modeshapes and their correlation for a center frequency of 11 Hz. The empirical modeshapes for those yeardays clearly do not match the WOA modeshapes, and that is supported by the correlation plots. It is not exactly known why these days do not produce good modeshapes, but we think that it might have something to do with the spikes at low frequencies in the PSD

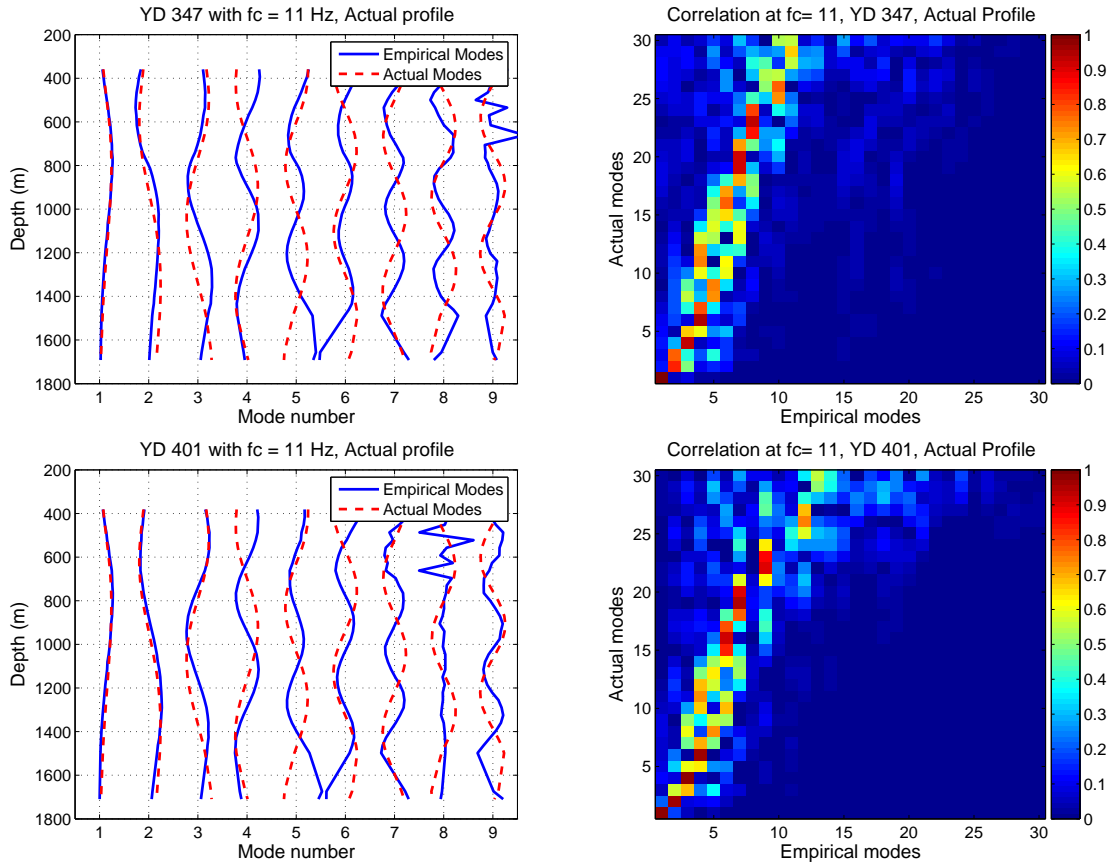


Figure 4.9: The extracted modes (shown in blue solid lines) at a center frequency of 11 Hz on yeardays 347 and 401 compared to the actual modes at those days computed from the environmental data (shown in red dashed line). On the right side of the figure the correlation between the modes plotted on the left.

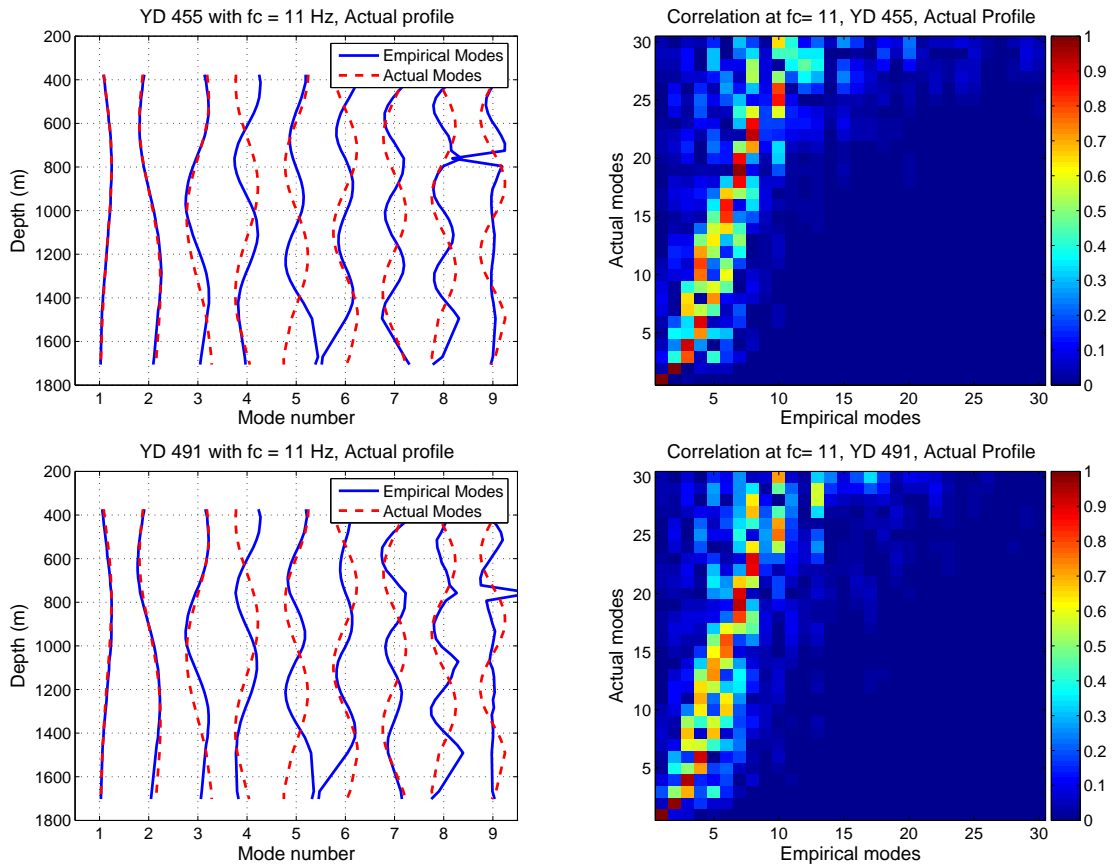


Figure 4.10: The extracted modeshapes (shown in blue solid lines) at a center frequency of 11 Hz on yeardays 455 and 491 compared to the actual modeshapes at those days computed from the environmental data (shown in red dashed line). On the right side of the figure the correlation between the modeshapes plotted on the left.

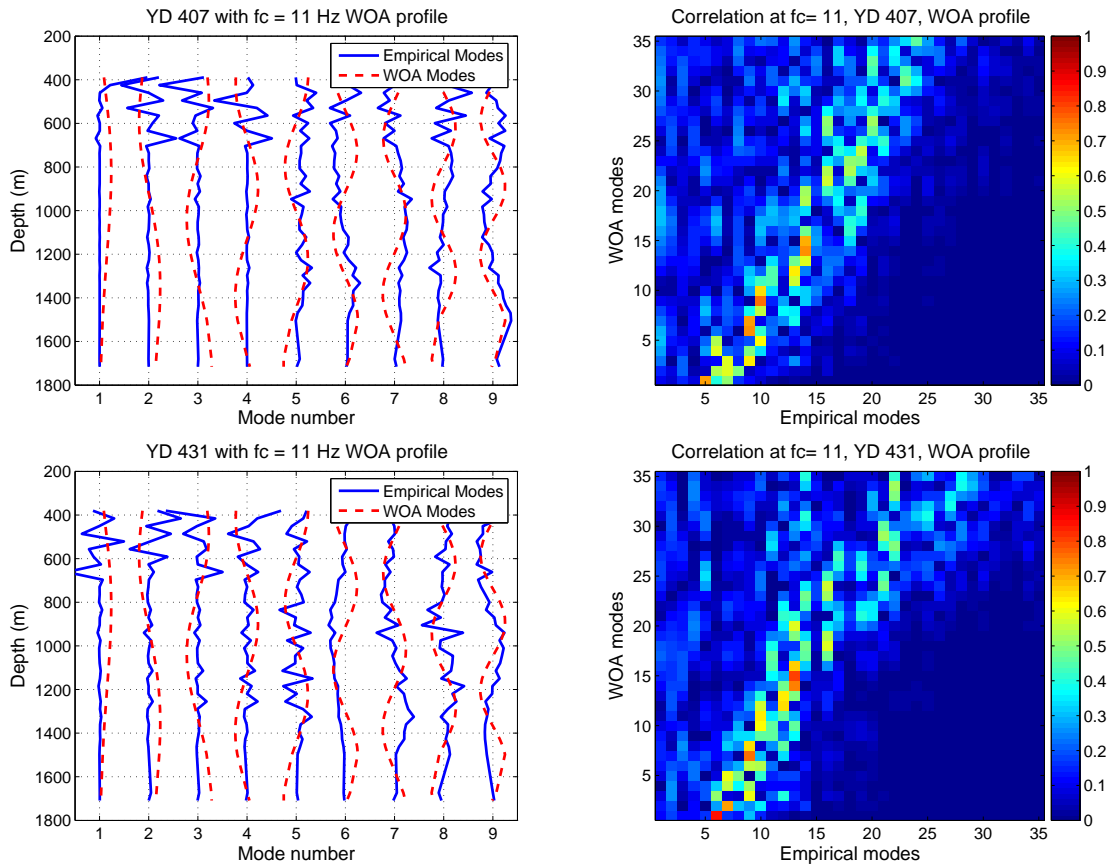


Figure 4.11: The extracted modeshapes (shown in blue solid lines) at a center frequency of 11 Hz on yeardays 407 and 431, where the extracted modeshapes do not look like modes, compared to the WOA modeshapes (shown in red dashed line). On the right side of the figure the correlation between the modeshapes plotted on the left.

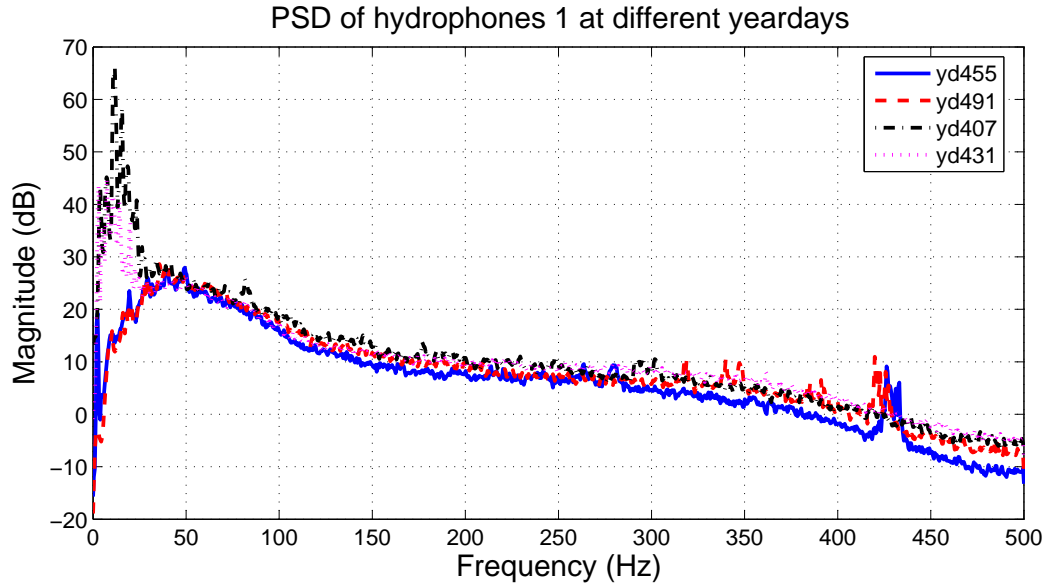


Figure 4.12: The figure shows the PSD of four yeardays at hydrophone 1. The yeardays shown are yearday 455 (shown in a blue solid line), yearday 491 (shown in a red dashed line), yearday 407 (shown in a black dash-dot line), and yearday 431 (shown in a dotted magenta line).

from the top hydrophone in Figure 4.5. Figure 4.12 shows the PSD of two days with “good” extraction (yearday 455 as a blue solid line and yearday 491 as a red dashed line) and two days with “bad” extraction (yearday 407 as a black dash-dot line and yearday 431 as a magenta dotted line). The figure shows high power at low frequency for the yeardays where the mode extraction is “bad”. In all the yeardays that produce modeshapes that look like the ones in Figure 4.11, the PSD of hydrophone 1 has high power at low frequencies. There are some yeardays where the PSD looks like the good yearday PSD. On those days the eigenvectors of $\hat{\mathbf{R}}$ have smooth shapes that look like modeshapes. For those yeardays the cause is not exactly known but may be caused by array tilt.

4.5 Summary

The SPICE04 dataset contains about 6 months worth of ambient noise measurements. The SVLA used in the experiment was strategically placed around the acoustic channel as shown in Figure 4.2, which makes it ideal for sampling normal mode arrivals. The SVLA also extensively sampled the environmental parameters of the ocean, such as temperature, salinity and pressure. These measurements enabled us to construct the SSP for a given day of the experiment. This is important because when comparing modeshapes it is ideal to compare them to the actual modes, rather than modes constructed from an averaged data set.

The empirical modes extracted from the received pressure field matched the actual modeshapes for the first 2 modes in some yeardays. This demonstrates that it is possible to use the method of eigendecomposition to extract the modes from pressure field receptions of ambient noise. For some yeardays the shapes of the eigenvectors of the CSDM did not look like modeshapes. The reason for this is not completely known, but we believe that it is caused by a localized loud source above the receiving array.

The PSD of ambient noise was taken over the duration of the experiment as shown in Figure 4.5. The figure shows the spikes, in the PSD for hydrophone 1, at low frequencies of what we believe is the localized high power source that causes the receptions that do not have good modeshapes extracted. Based on the SPICE04 analysis, we believe the PSD of noise for the top hydrophone is associated with the failure of this mode extraction method.

Chapter 5: Conclusion

A discussion of the method of extracting the modeshapes from ambient noise measurements is now presented in this chapter. A summary of simulation results, the results obtained from the SPICE04 experiment, and a conclusion about the performance of the method is discussed in section 5.1. Section 5.2 discusses proposed future work that will build on the work presented in this thesis, including a further analysis of the effect of windstress on the receptions over the period of the experiment and inversion for environmental parameters from the extracted modeshapes.

5.1 Concluding comments

Previous work demonstrated that eigendecomposition of the CSDM constructed using pressure field measurements can produce a good estimate of the propagating modeshapes without prior knowledge of the sound speed. This thesis tested the method using simulations and measured data from the SPICE04 experiment. The receptions from the SVLA were analyzed and the extracted modeshapes compared to the modeshapes computed from the measured SSP. Environmental data, such as temperature, salinity and pressure, were extensively sampled during the experiment, which allowed for the actual SSP to be computed at any yearday thus the actual modeshapes can be generated for any yearday.

The extraction method was first demonstrated in simulations of the narrow-band pressure field receptions to study the limits of the method in deep water environments. Simulations compared the performance for a water-column-spanning array

and the SVLA deployed in the SPICE04 experiment. The effect of array tilt on the extracted modes was studied in simulations as well. The simulations demonstrated that it is possible to use this method if the following two criteria are met. First the receiving VLA must densely sample the complete water column in order to extract the modeshapes properly. The second criteria, confirmed in this thesis, is that the variance of adjacent amplitude weights (or the eigenvalues of the CSDM) for each mode should be at least 5% to 10% apart as introduced in [3]. If the first criteria cannot be met in deep water environments, the array should be positioned around the acoustic channel axis or the minimum sound speed, because the low order modeshapes are centered around the minimum sound speed. The array should also be long enough to capture the modeshapes and the spacing between elements depends on the frequency. As noted in Chapter 2, the modes are frequency dependent. As the frequency increases the modeshapes become more compact in depth and can be sampled by a shorter array, but the distance between elements may also need to be smaller.

The simulation results in Section 3.2 showed that at 11 Hz the maximum number of good modes extracted are two. The reason is that the array was designed to sample modes at frequencies higher than 11 Hz. At 11 Hz when the mode number increases the modeshapes span depths longer than the sampling range of the array, therefore only the modes that show completely in the sampling depths of the array can be extracted.

The modeshapes from the measured data were extracted at several frequencies from ambient noise measurements, as shown in Figure 4.8, which shows that the highest center frequency that provided good low order modes is 11 Hz. At that frequency the results from extracting the modeshapes were similar to the ones in Section 3.2, where only the first two modes can be extracted. Comparing the performance of the

method in deep water to shallow water, the results are similar in the sense that they were able to only extract a couple of modes and the same is demonstrated in this thesis for a deep water environment.

Overall this thesis demonstrated that it is possible to extract normal modes in deep water environments from ambient noise receptions using no prior knowledge of the environmental parameters. An important contribution of this work is the comparison to the “true” modeshapes generated from the measured environmental data. Previous work did not include such comparisons.

5.2 Future work

As noted at the end of Chapter 4 there are some receptions where the technique of extracting the modes returned vectors that did not look like anything resembling modeshapes. Based on the SPICE04 analysis, the PSD of noise for the top hydrophone is associated with the failure of the eigendecomposition mode extraction method. We believe that there might be correlation between the receptions during those yeardays and the windstress at that time directly above the SVLA. High windstress data suggests that there is a storm present above the SVLA. If most noise is due to a storm at the surface, the source is not distant, thus the assumption of uncorrelated modes is violated. We would not expect the mode extraction method to work well under these conditions. A direct correlation was not found when the raw data is compared to the windstress data. Since the source of windstress is from the surface of the ocean, if we were to beamform the receptions for all yeardays to look towards the surface of the ocean, then that should yield a more accurate correlation. For future work beamforming will be implemented on the data and compared to the windstress.

Other future work includes the inversion for the environmental parameters,

i.e., sound speed, from the extracted modeshapes, as presented in previous work by Neilsen and Westwood [3,6]. Inverting for the environmental parameters would make work much easier to implement acoustic tomography when only pressure field measurements are available.

Bibliography

Bibliography

- [1] W. Munk, P. Worcester, and C. Wunsch, *Ocean Acoustic Tomography*. New York: Cambridge University Press, 1995.
- [2] T. Boyer, J. Antonov, H. Garcia, D. Johnson, R. Locarnini, A. Mishonov, M. Pitcher, O. Baranova, and . I.V. Smolyar, “World Ocean Database 2005. S. Levitus, Ed.” in *NOAA Atlas NESDIS 60*, U.S. Government Printing Office, Washington, D.C., pp. 190, DVDs.
- [3] T. B. Neilsen and E. K. Westwood, “Extraction of acoustic normal mode depth functions using vertical line array data,” *Journal of the Acoustical Society of America*, vol. 111, pp. 748–756, 2002.
- [4] S. N. Wolf, D. K. Cooper, and B. J. Orchard, “Environmentally adaptive signal processing in shallow water,” in *Proc. IEEE OCEANS’93. ‘Engineering in Harmony with Ocean’*, Victoria, BC, Canada, Oct. 1993, pp. 99–104.
- [5] P. Hursky, W. S. Hodgkiss, and W. A. Kuperman, “Matched field processing with data-derived modes,” *Journal of the Acoustical Society of America*, vol. 109, pp. 1355–1366, 2001.
- [6] T. B. Neilsen, “Normal mode extraction and environmental inversion from underwater acoustic data,” Ph.D. dissertation, University of Texas at Austin, Austin, May 2000.
- [7] F. B. Jensen, W. A. Kuperman, M. B. Porter, and H. Schmidt, *Computational Ocean Acoustics*. New York: Springer-Verlag New York, Inc., 2000.
- [8] R. J. Urick, *Principles of Underwater Sound*. New York: McGraw-Hill Inc., 1975.
- [9] G. M. Wenz, “Acoustic ambient noise in the ocean: Spectra and sources,” *Journal of the Acoustical Society of America*, vol. 34, pp. 1936 – 1956, 1962.
- [10] H. Medwin and Colleagues, *Sounds in the Sea*. Cambridge: Cambridge University Press, 2005.
- [11] W. W. L. Au, *The sonar of dolphins*. New York: Springer-Verlag, 1993.

- [12] W. A. Kuperman and F. Ingenito, “Spatial correlation of surface generated noise in a stratified ocean,” *Journal of the Acoustical Society of America*, vol. 67, pp. 1988–1996, 1980.
- [13] J. S. Perkins, W. A. Kuperman, F. Ingenito, and L. T. Fialkowski, “Modeling ambient noise in three-dimensional ocean environments,” *Journal of the Acoustical Society of America*, vol. 93, pp. 739–752, 1993.
- [14] G. L. D’Spain, L. P. Berger, W. A. Kuperman, J. L. Stevens, and G. E. Baker, “Normal mode composition of earthquake T phases,” *Pure and Applied Geophysics*, vol. 158, pp. 475–512, 2001.
- [15] G. H. Golub and C. F. V. Loan, *Matrix Computations*, third edition ed. Baltimore: The Johns Hopkins University Press, 1996.
- [16] I. S. Reed, J. D. Mallett, and L. E. Brennan, “Rapid convergence rate in adaptive arrays,” *IEEE Transactions on Aerospace and Electronic Systems*, vol. AES-10, pp. 853 – 863, 1974.
- [17] A. V. Oppenheim, R. W. Schaffer, and J. R. Buck, *Discrete-Time Signal Processing (Second Edition)*. New Jersey: Prentice-Hall Signal Processing Series, 1999.

Curriculum Vitae

Khalid Almuhanha was born in Riyadh, Saudi Arabia on October 15, 1983 and lived there for the first 12 years of his life. He has been living in the United States since 1995. He finished High School in 2001. He started his Undergraduate studies at George Mason University (GMU) in the Fall of 2001. He started his Graduate studies also at GMU in the Fall of 2005.

During his master's program, Khalid started working as a Teacher's Assistant (TA) during the Spring 2006 semester. Since the Summer of 2006 he has been working with Dr. Kathleen Wage as a Research Assistant (RA), working on two projects; the Signals and Systems Concept Inventory (SSCI) and the work presented in this thesis.

Khalid got accepted into the Ph.D. program at GMU during the Spring 2008 semester. His future hopes after completing his Ph.D. is to become a professor and do research at a university.